Soft Matter

Light Scattering from Mixtures of Interacting, Nonionic Micelles with Hydrophobic Solutes

Journal:	*Soft Matter*
Manuscript ID	SM-ART-07-2022-001007.R1
Article Type:	Paper
Date Submitted by the Author:	08-Nov-2022
Complete List of Authors:	Alexander, Nathan; University of Delaware, Chemical and Biomolecular Engineering Phillips, Ronald; University of California Davis, Chemical Engineering Dungan, Stephanie; University of California Davis, Chemical Engineering; University of California Davis, Food Science and Technology

ARTICLE

Light Scattering from Mixtures of Interacting, Nonionic Micelles with Hydrophobic Solutes

Nathan P. Alexander,*[a] Ronald J. Phillips,[b] and Stephanie R. Dungan[b,c]

Model equations for the Rayleigh ratio and the electric field autocorrelation function are derived using thermodynamic fluctuation theory applied to crowded solute-containing micellar solutions and microemulsions with negligible molecular species and polydispersity. This theory invokes non-equilibrium thermodynamics and enforces local equilibrium between molecular solute, surfactant, and the various micellar species, in order to elucidate the influence of self-assembly on light scattering correlation functions. We find that self-assembly driven variations in the average micelle radius and aggregation number along gradients in concentration, which were previously shown to drive strong multicomponent diffusion effects expressed via the ternary diffusivity matrix [$\mathbf{D}$], do not affect the scattering functions in the limit of zero local polydispersity. Hence, theoretical predictions for the Rayleigh ratio and the field autocorrelation function for ternary mixtures of solute-containing, locally monodisperse micellar solutions are identical to those developed for binary mixtures of monodisperse, colloidal hard spheres. However, self-assembly driven multicomponent diffusion phenomena are predicted to influence the thermodynamic driving forces for diffusion in these mixtures. In support of our theoretical results, measurements for the Rayleigh ratio and the field autocorrelation function for ternary aqueous solutions of decaethylene glycol monododecyl ether ($C_{12}E_{10}$) with either decane or limonene solute were performed for several molar ratios and volume fractions up to $\phi \approx 0.25$, and for binary mixtures of $C_{12}E_{10}$/water up to $\phi \approx 0.5$. Excellent agreement between our light scattering theory and experimental data is achieved for low to moderate volume fractions ($\phi < 0.3$), and at higher concentrations when our theoretical results are corrected to account for micelle dehydration.

1 Introduction

According to the Onsager regression hypothesis,[1, 2] microscopic fluctuations in the thermodynamic variables of a multicomponent fluid, such as temperature, pressure, and the species concentrations, relax, on average, by the same transport equations that govern the relaxation of macroscopic gradients. For small departures from equilibrium, the independent diffusive fluxes for $n-1$ components in an n-component liquid mixture, at constant temperature and pressure, may be described by the generalized form of Fick's law:

$$\boldsymbol{J}_i = -\sum_{j=1}^{n-1} D_{ij} \boldsymbol{\nabla} C_j$$

$$for\ i\ =\ 1,2,\ldots,n-1\ . \qquad (1)$$

Here, D_{ij} is an element of the diffusivity matrix that relates the flux $\boldsymbol{J}_i$ of component i to a concentration gradient $\boldsymbol{\nabla} C_j$ in component j. Non-zero cross diffusivities $D_{ij}(j \neq i)$, indicate multicomponent diffusion coupling phenomena resulting from interactions between different diffusing species. Since concentration fluctuations also cause an irradiated mixture to scatter light, the same multicomponent diffusion phenomena observed during a macro-gradient experiment, such as the Taylor dispersion[3-5] or interferometric methods,[6, 7] are expected to influence the correlation functions used to model light scattering data acquired via photon correlation and time averaged spectroscopy.

Recent studies on multicomponent diffusion in nonionic micellar solutions[6, 8, 9] and water-in-oil microemulsions[10, 11] indicate strong multicomponent effects, including strong uphill diffusion, driven by solubilization-induced micelle growth that drives surfactant up a solute gradient. However, these effects appear to be absent in measurements of the field autocorrelation function and the Rayleigh ratio, which, surprisingly, conform to theory for binary mixtures of colloidal hard spheres.[8, 12, 13] The main goal of this article is to present a rigorous derivation for the field autocorrelation function and the Rayleigh ratio for ternary surfactants solutions with hydrophobic solutes in the limit of local monodispersity. This derivation explains the observation that multicomponent diffusion phenomena, which strongly affect the diffusivity matrix, negligibly affect the light scattering functions for aqueous mixtures of nonionic micelles and hydrophobic solutes.

Theoretical results[14-18] for the field autocorrelation function and the Rayleigh ratio for polydisperse mixtures of rigid, colloidal hard spheres have been derived, mainly to examine

[a] Department of Chemical and Biomolecular Engineering, University of Delaware, Newark, DE 91716 USA. Email: npalex@udel.edu
[b] Department of Chemical Engineering, University of California at Davis, Davis, CA 95616 USA.
[c] Department of Food Science and Technology, University of California at Davis, Davis, CA 95616 USA

the influence of optical and size polydispersity on the intensity of scattered light. Some of these models were later extended to apply to ternary mixtures of solute-containing micelles, modelled as immutable, colloidal spheres with a core-shell morphology.[19, 20] However, self-assembled surfactant solutions differ fundamentally from dispersions comprised of discrete, rigid particles, since micelles may grow and change shape as they diffuse, re-equilibrating locally to variations in temperature, pressure, and composition along their diffusion path. Hence, one may question whether light scattering theory developed for mixtures of discrete colloidal scatterers with fixed shapes and sizes, which does not account for the effects of self-assembly during light scattering measurements, is applicable to multicomponent surfactant solutions.

In order to capture the influence of self-assembly on light scattered from solute-containing micellar solutions, fluctuation theory[21-36] is used here to derive the field autocorrelation function and the Rayleigh ratio for this system. Per this framework, surfactant solutions are modelled as a continuous medium comprised of solute (a), surfactant (s), and solvent (w) that self-assemble on a time scale much faster than that of diffusion, thereby satisfying the local equilibrium assumption of irreversible thermodynamics.[37] Here, local equilibrium is enforced by the Gibbs-Duhem equation, which provides equilibrium relations between the chemical potentials of free solute, surfactant monomer, and the various micelle species. Thus, chemical potential gradients in solute and surfactant are related to gradients in the micelle species chemical potentials, which drive diffusive transport governed by rigorous theory by Batchelor[38-40] for polydisperse colloidal hard sphere dispersions. At the continuum level, the resulting diffusion of solute and surfactant relaxes fluctuations in the composition-dependent, local dielectric constant of the solution, which determines the intensity of scattered light at low wave vectors satisfying $qR_{i^*} \ll 1$. Here, $q = 4\pi n/\lambda_0 sin(\theta/2)$ is the magnitude of the wave vector, n is the refractive index of the solution, λ_0 is the wavelength of incident light, θ is the scattering angle, and R_{i^*} is the average micelle radius.

Currently, only a few studies have evaluated the mode amplitudes predicted by thermodynamic fluctuation theory to analyze dynamic light scattering (DLS) data for multicomponent mixtures that contain surfactants and are far from a phase boundary or critical point.[20, 41-44] Notably, semi-empirical calculations for the mode amplitudes of the field autocorrelation function for dilute SDS/NaCl/water mixtures[42] and mixed zwitterionic surfactant solutions,[41] were performed using a combination of experimental data and dilute theory, for which interparticle interactions were neglected, to estimate the chemical potential derivatives, the ternary diffusion coefficients, and the refractive index increments. For aqueous systems, only a single mass diffusion mode was observed, even though two modes are generally predicted for ternary mixtures. In most cases, the mode amplitude calculations indicated the dominant mode corresponds to the lower eigenvalue, in agreement with experimental data.[41, 42, 45] By comparison, the field autocorrelation function derived in this work for concentrated mixtures of interacting, solute-containing micelles, rigorously reduces to monomodal decay according to the larger eigenvalue.

In the following sections we introduce equilibrium data that establishes strong micellar growth with respect to composition for aqueous, mixtures of $C_{12}E_{10}$ micelles with limonene. Next, thermodynamic fluctuation theory is reviewed and applied to derive both the Rayleigh ratio and the field autocorrelation function for ternary mixtures. Thermodynamic derivatives for the solute and surfactant are then derived for ternary micellar solutions, followed by derivations for the scattering functions applied to solute-containing micellar solutions for a variety of limiting special cases. This work concludes with a comparison and validation of our locally monodisperse theory, in which local polydispersity is neglected but variations in the local, average micelle radius and aggregation number (micelle growth effects) are retained, with our experimental data.

2 Materials and Methods

2.1 Materials

Nonionic surfactant decaethylene glycol monododecyl ether ($C_{12}E_{10}$, lot #SLBT1187 or #0000057654 each with a hydroxyl value equal to 92.0 mg/g), the hydrophobic solutes decane and limonene, and HPLC grade toluene (used as a reference standard for static light scattering measurements), were all purchased from Sigma-Aldrich and used without modification. “Molecular Biology Reagent” water from Sigma-Aldrich (filtered through 0.1 µm filters by the manufacturer) was used to mix solutions for light scattering measurements. All mixtures were prepared by volume with aliquots from 100 mL stock solutions and were allowed to equilibrate overnight at room temperature. Non-ideal changes in volume upon mixing were neglected.

2.2 Light Scattering

Dynamic (DLS) and static (SLS) light scattering measurements were performed at 25 °C using either a Malvern Zetasizer Nano ZS90 or Malvern Ultra at a 90° scattering angle. The light source was a solid state 4 mW He-Ne laser that emitted vertically polarized light with a wavelength equal to $\lambda_0 = 633nm$ and a scattering vector $q = 4\pi n/\lambda_0 sin(\theta/2) \cong 0.002\ \text{Å}^{-1}$. In this study, the average micelle radii did not exceed $5nm$. Hence, $qR_{i^*} = 4\pi nR_{i^*}/\lambda_0 sin(\theta/2) < 0.1 \ll 1$, in reasonable satisfaction of the low wave vector criterion for the application of thermodynamic fluctuation theory to the analysis of light scattering data.To ensure the removal of dust particles, all surfactant solutions prepared for light scattering measurements were filtered through 0.1 µm Whatman polycarbonate filters (model WHA800309), using an Avanti mini-extruder (model 610000), directly into quartz cuvettes topped with Teflon stoppers by Starna (model 23-Q-10). Each 1mL sample was then allowed to equilibrate at 25 °C within the instrument for several minutes prior to measurement. For each DLS measurement, monomodal or nearly monomodal decay of the field autocorrelation function was observed for all samples. Hence, the method of cumulants was used to acquire diffusion coefficients (D_{DLS}) and polydispersity indices.

SLS measurements yielded excess Rayleigh ratios R_θ, at scattering angle θ, calculated using[46]

$$R_\theta = \left(\frac{n}{n_T}\right)^2 R_T \frac{\langle I_a(0)\rangle}{\langle I_T(0)\rangle} \quad . \qquad (2)$$

Here, $n_T(=1.496)$, $R_T(=1.3522 \times 10^{-5} cm^{-1})$, and $\langle I_T(0)\rangle$ are the refractive index, Rayleigh ratio, and time averaged scattering intensity, respectively, of the reference standard toluene at 25 °C. $\langle I_a(0)\rangle$ is the residual scattering intensity, defined as the difference between the scattering intensity of the solution and that of the pure solvent, and n is the solution refractive index, which was assumed to vary linearly according to $n = (\partial n/\partial c_s)_{p,T,C_a/C_s} c_s + n_0$. The refractive index derivatives $(\partial n/\partial c_s)_{p,T,C_a/C_s}$ were independently measured using a differential refractometer (Waters model 2414) at room temperature (23.0 ± 0.3 °C) by varying the surfactant mass concentration c_s, and $n_0 = 1.33$ is the refractive index of pure water at 25 °C.

To evaluate the derivatives , the solution refractive index n was measured relative to the solvent n_0 from a dilution series of six different surfactant concentrations that ranged from 1–6 mM in increments of 1 mM, with the solute to surfactant molar ratio C_a/C_s held constant. For the limonene system, $(\partial n/\partial c_s)_{p,T,C_a/C_s}$ values were then determined from the slopes of the plots of $(n - n_0)$ versus c_s for the following molar ratios: C_a/C_s = 0, 0.1, 0.2, 0.3, and 0.5. Each plot was reproduced in triplicate and was well fit with a linear function with an intercept through zero. This procedure yielded values for dn/dc_s equal to 0.1314 ± 0.0006, 0.133 ± 0.001, 0.1372 ± 0.0007, 0.140 ± 0.001 and 0.1491 ± 0.0005 mL/g, respectively. Derivatives $(\partial n/\partial c_s)_{p,T,C_a/C_s}$ used for the decane system were obtained from an earlier study.[8]

Except where noted, all reported error bars for our scattering measurements represent two standard deviations.

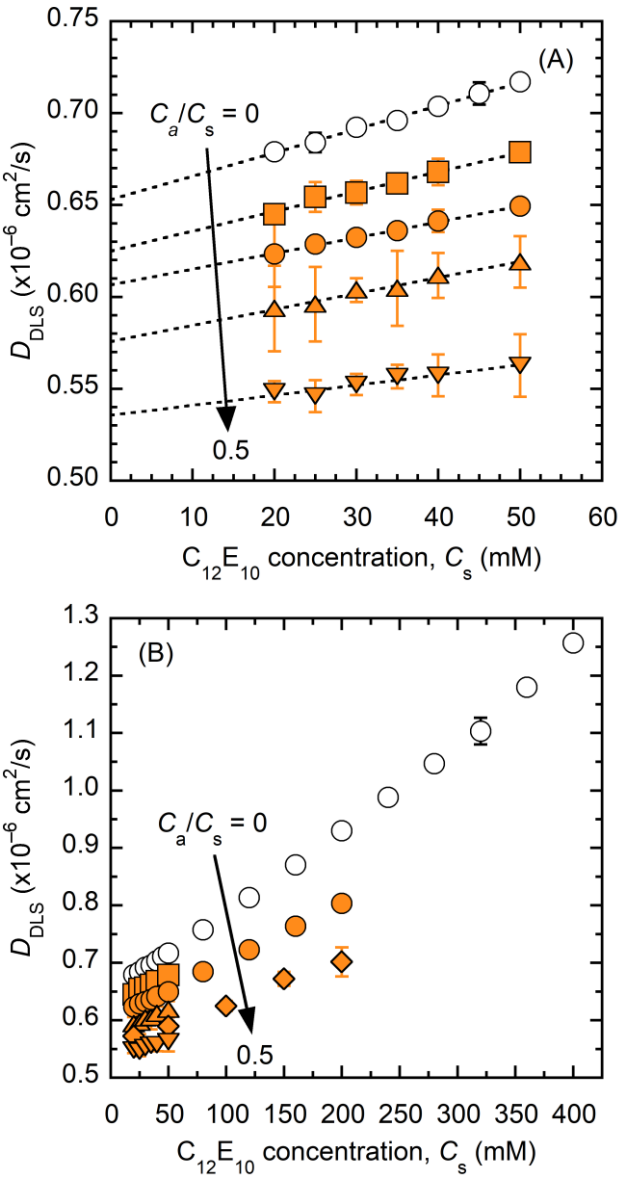

Fig. 1 (A) DLS diffusion coefficients for aqueous $C_{12}E_{10}$ (s) + limonene (a) for $C_a/C_s = 0,\ 0.10,\ 0.20,\ 0.30,$ and 0.50 plotted versus surfactant concentration over $0\ mM \le C_s \le 50\ mM$ and (B) for concentrated mixtures with $C_a/C_s = 0, 0.10, 0.20, 0.30, 0.36,$ and 0.50 up to $C_s = 400\ mM$.

3 Results

3.1 Dynamic light scattering (DLS)

Diffusion coefficients D_{DLS} for ternary $C_{12}E_{10}$/limonene/water mixtures are shown in Fig. 1 with constant molar ratios $C_a/C_s = 0, 0.10, 0.20, 0.30,$ or 0.50, and surfactant concentrations that ranged from 20 mM to 400 mM. The D_{DLS} values reported here, and in previous work for $C_{12}E_{10}$/decane/water mixtures,[8] were acquired using the method of cumulants. The latter were shown consistent with the theory of Batchelor for gradient diffusion of monodisperse hard spheres.[38]

3.2 Static light scattering (SLS)

In Fig. 2A, reduced scattering intensities $K_s c_s/R_{90}$ for dilute, aqueous $C_{12}E_{10}$(s)/limonene(a) mixtures are plotted versus surfactant mass concentration c_s with constant molar ratios $C_a/C_s = 0, 0.1,\ 0.2,\ 0.3,$ and 0.5. Here, $K_s = 4\pi^2 n^2/\left(N_A {\lambda_0}^4\right)(\partial n/\partial c_s)^2_{p,T,C_a/C_s}$ is the optical contrast constant and N_A is Avogadro's number. As shown, $K_s c_s/R_{90}$ increased linearly for each molar ratio. This behavior indicates that, with constant C_a/C_s, the micelles did not grow or change shape with increasing surfactant concentration, thus validating extrapolation of the data to determine MW_s as presented below. In Fig. 2B, R_{90} values for concentrated $C_{12}E_{10}$/water, and for $C_{12}E_{10}$/limonene/water and $C_{12}E_{10}$/decane/water solutions with constant molar ratios equal to $C_a/C_s = 0.2$, are plotted against the molar surfactant concentration C_s. The R_{90} values were calculated using eqn (2), for which no assumptions were made regarding the shape, size distribution, hydration, or interparticle interactions.

3.3 Micelle structure at infinite dilution

DLS diffusion coefficients (Fig. 1) and reduced scattering intensities (Fig. 2A) were extrapolated to zero surfactant concentration to determine the diffusion coefficient D^0_{DLS} and the molecular weight of surfactant per micelle MW_s at infinite dilution for each molar ratio C_a/C_s. Assuming the micelles were

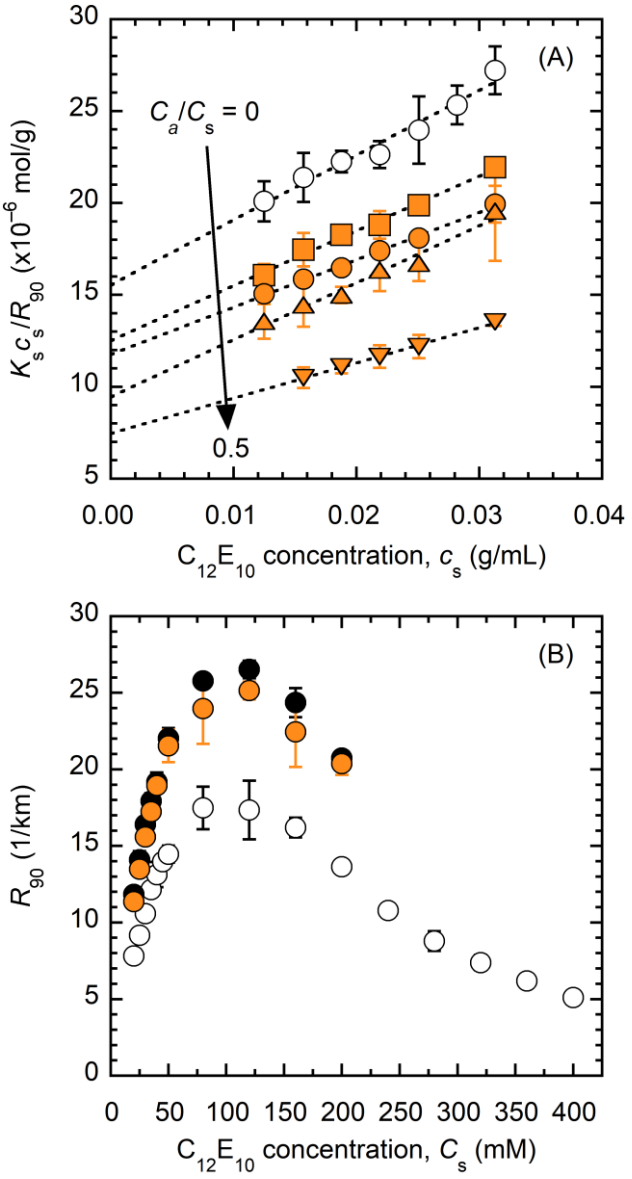

Fig. 2 (A) Reduced scattering intensities with respect to $C_{12}E_{10}$ (s) concentration with $C_a/C_s = 0$, 0.10, 0.20, 0.30, and 0.50 for dilute $C_{12}E_{10}$/limonene/water mixtures and (B) Rayleigh ratios for concentrated $C_{12}E_{10}$/water (white), and $C_{12}E_{10}$/decane/water (black) and $C_{12}E_{10}$/limonene/water (orange) mixtures with $C_a/C_s = 0.2$.

spherical, the micelle hydrodynamic radius R_{DLS} for each C_a/C_s was calculated using the Stokes-Einstein equation,

$$R_{DLS} = \frac{k_B T}{6\pi\eta D^0_{DLS}} \quad . \qquad (3)$$

Here, k_B is Boltzmann's constant, T is temperature, and η is the solvent viscosity (0.89 mPa·s at 25 °C). The micelle aggregation number $\bar{m}$ was calculated by dividing MW_s by the molecular weight of $C_{12}E_{10}$ (626.86 g/mol). The evaluation of the molecular weight of surfactant within micelles MW_s is explained in our earlier work,[8] and is also elaborated in developing eqn (123) below. Using the experimentally determined values for R_{DLS} and $\bar{m}$, the micelle hydration indices n_H, defined as the average

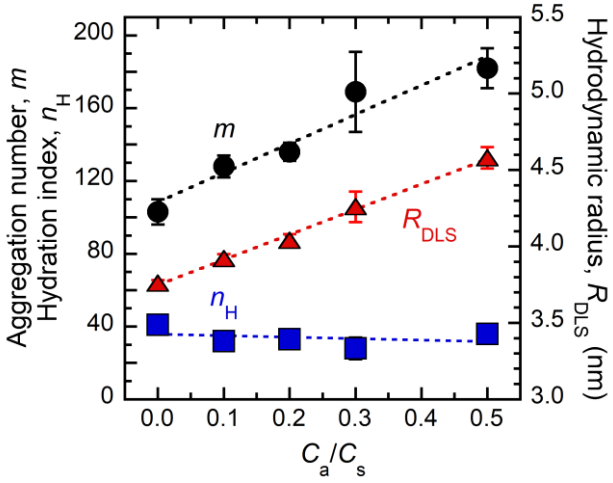

Fig. 3 Aggregation numbers $\bar{m}$ from SLS data, hydrodynamic radii R_{DLS} from DLS data, and hydration indices n_H with respect to molar ratio C_a/C_s for aqueous $C_{12}E_{10}$ (s) + limonene (a) at infinite dilution. Error bars indicate 95% confidence intervals.

number of water molecules bound to each surfactant molecule within the micelle, were estimated by calculating the difference between the measured hydrated volume of a solute-containing micelle $\left(4/3\,\pi {R_{DLS}}^3\right)$ and its empirically determined dry volume $(\bar{m}V_s + \bar{n}V_a)$:

$$n_H = \frac{4/3\,\pi {R_{DLS}}^3 - \bar{m}V_s - \bar{n}V_a}{\bar{m}V_w} \quad . \qquad (4)$$

Here, V_s, V_a, and V_w are the respective molecular volumes of a dry molecule of $C_{12}E_{10}$ (0.99 nm^3), limonene (0.27 nm^3), and water (0.03 nm^3), and $\bar{n} = \bar{m}\,C_a/C_s$ is the average number of solute molecules per micelle. V_a and V_w were calculated from the pure liquid densities of limonene and water, respectively, at 25 °C and V_s was interpolated from density data acquired for a homologous series of aqueous $C_{12}E_m$ surfactant solutions.[47]

In Fig. 3, R_{DLS}, $\bar{m}$, and n_H for aqueous $C_{12}E_{10}$/limonene solutions are plotted versus C_a/C_s. As shown, R_{DLS} and $\bar{m}$ both increased with increasing C_a/C_s, indicating that $C_{12}E_{10}$ micelles grew via the added volume of both limonene and hydrated $C_{12}E_{10}$ surfactant. The trend in R_{DLS} with limonene concentration is consistent with results by others for aqueous solutions of $C_{16}E_{10}$/limonene via DLS.[48] Furthermore, n_H remained approximately constant, indicating that limonene, which is expected to solubilize within the hydrophobic core of the micelles, had little effect on the PEG/water composition within the micelle shell. Similar results were observed previously by us for aqueous $C_{12}E_{10}$/decane mixtures.[8] Furthermore, our solute-free aggregation number ($m_0 = 103 \pm 7$), hydrodynamic radius ($R_{DLS} = 3.76 \pm 0.02\ nm$), and hydration index ($n_H = 41 \pm 5$), agree with our previous results.[8] Using $n_H = 40$ in accordance with Fig. 3, one finds that the volume $\bar{m}n_H V_w$ occupied by hydration water within each $C_{12}E_{10}$ micelle is significant, accounting for roughly half of the total volume per micelle. Furthermore, the micelle growth rate $a_1 = 1.56\ nm$ for limonene-containing micelles was determined from the slope of the plot of R_{DLS} versus C_a/C_s.

4 Theory

4.1 Development of light scattering correlation functions for ternary mixtures

4.1.1 Thermodynamic fluctuation theory

Following Berne and Pecora,[22] a liquid mixture within the sample cuvette of a light scattering apparatus is modelled as a composite thermodynamic system, where a subsystem A, representing the illuminated region of the solution with scattering volume V, exists within a much larger bath B, representing the remaining liquid of the sample. Mass and energy may exchange between subsystems A and B, but the total composite system is assumed isolated overall. Consequently, the probability for a particular fluctuation in A is given by Boltzmann's equation

$$P(\delta \boldsymbol{x}) = {\Omega_0}^{-1} exp\left(\frac{\delta S_T}{k_B}\right) \ . \tag{5}$$

Here, Ω_0 is a normalization constant, $\delta \boldsymbol{x}$ is a fluctuation in a vector of thermodynamic variables, and $P(\delta \boldsymbol{x})$ is the fluctuation probability.

For small disturbances, the total entropy fluctuation δS_T of a ternary mixture comprising the composite thermodynamic system is given by

$$\delta S_T = -\frac{1}{2T}\left(\delta T \delta S - \delta p \delta V + \sum_{i=1}^{3} \delta \mu_i \delta N_i\right) \ . \tag{6}$$

In eqn (6), S is entropy, μ_i are the species chemical potentials, p is pressure, and N_i is the number of moles of species i in subsystem A. During a typical light scattering experiment, the scattering volume is fixed ($\delta V = 0$). Furthermore, temperature and pressure fluctuations are neglected in this study, so that $\delta T = \delta p = 0$ and eqn (6) becomes

$$\delta S_T = -\frac{1}{2T}\left(\sum_{i=1}^{3} \delta \mu_i \delta N_i\right) \ . \tag{7}$$

It is desirable to re-express eqn (7) in terms of concentration fluctuations, and to eliminate the contribution from the solvent. Using the constant volume constraint and the Gibbs-Duhem equation, one can show (see section 1.1 of Supplementary Information (SI))

$$\sum_{i=1}^{3} \delta \mu_i \delta N_i = V \sum_{i=1}^{2} \sum_{k=1}^{2} G_{ik} \delta C_i \delta C_k = V \delta \boldsymbol{C}^T \cdot [\boldsymbol{G}] \cdot \delta \boldsymbol{C} \ , \tag{8}$$

where the superscript T indicates the transpose of the molar concentration vector $\boldsymbol{C}$. The elements of the matrix $[\mathbf{G}]$ are given by (see section 1.1 of SI)

$$G_{ik} = \left(\frac{\partial \mu_i}{\partial C_k}\right)_{T,\mu_n,V,C_{i\neq k}} = \left(\frac{\partial \mu_i}{\partial C_k}\right)_{p,T,C_{i\neq k}} + \frac{\bar{V}_i}{1-\phi} \sum_{j=1}^{2} C_j \left(\frac{\partial \mu_j}{\partial C_k}\right)_{p,T,C_{i\neq k}}$$
$$for\ i,k = 1,2 \ , \tag{9}$$

and the chemical potentials are defined as

$$\mu_i = \left(\frac{\partial \tilde{F}}{\partial N_i}\right)_{T,\mu_n,V,N_{k\neq i}} = \left(\frac{\partial g}{\partial N_i}\right)_{p,T,N_{k\neq i}} \quad for\ i,k = 1,2, \tag{10}$$

where $\tilde{F}$ and g are the extensive McMillan-Mayer[49, 50] and Gibbs free energies, respectively. For the remainder of this article, we will abbreviate the subscripts $T, \mu_n, V, N_{k\neq i}$ and $p, T, N_{k\neq i}$ as T, μ_n and p, T, respectively.

In order to decouple the concentration fluctuations in eqn (8), we follow Bardow[21] and define a modal matrix $[\mathbf{P}]$ for the diffusion coefficient matrix $[\mathbf{D}]$, which is constructed with column vectors equal to the eigenvectors for $[\mathbf{D}]$. The result is used to diagonalize $[\mathbf{G}]$ via (see section 1.2 of SI)

$$\left[\hat{\mathbf{G}}\right] = [\mathbf{P}]^{\mathrm{T}}[\mathbf{G}][\mathbf{P}] \ , \tag{11}$$

satisfying the Onsager symmetry relation,[1, 2] where the matrix $[\mathbf{P}]$ is given by

$$\begin{bmatrix} P_{11} & P_{12} \\ P_{21} & P_{22} \end{bmatrix} = \begin{bmatrix} 1 & \left(\frac{D_{12}}{D_+ - D_{11}}\right) \\ \left(\frac{D_- - D_{11}}{D_{12}}\right) & 1 \end{bmatrix} \ , \tag{12}$$

and the eigenvalues of the diffusivity matrix are

$$D_- = \frac{(D_{11} + D_{22})}{2} - \frac{\sqrt{(D_{11} - D_{22})^2 + 4D_{12}D_{21}}}{2} \tag{13}$$

and

$$D_+ = \frac{(D_{11} + D_{22})}{2} + \frac{\sqrt{(D_{11} - D_{22})^2 + 4D_{12}D_{21}}}{2} \ . \tag{14}$$

Eqn (5), and (7)–(11) yield a Gaussian distribution function

$$P(\delta \boldsymbol{x}) = {\Omega_0}^{-1} exp\left\{-\frac{V}{2k_B T}\left(\sum_{i=1}^{2} \hat{G}_i \delta {\hat{C}_i}^2\right)\right\} \ , \tag{15}$$

with variances defined according to (see section 1.3 of SI)

$$\langle \delta {\hat{C}_i}^2 \rangle = \frac{k_B T}{V \hat{G}_i} \ . \tag{16}$$

Here, $\hat{G}_i$ are the diagonal elements of $\left[\hat{\mathbf{G}}\right]$, $\hat{C}_i$ are elements of the transformed concentration vector $\left[\hat{\mathbf{C}}\right]$, defined via $[\mathbf{C}] = [\mathbf{P}] \cdot \left[\hat{\mathbf{C}}\right]$, and the angle brackets $\langle\ \ \rangle$ denote ensemble averages. Eqn (16) describes the mean-square of independent, linear combinations of species concentration fluctuations at equilibrium and is used to derive both the field autocorrelation function and the Rayleigh ratio for ternary micellar solutions in the following sections.

4.1.2 Normalized time autocorrelation function $\left|\boldsymbol{g}^{(1)}(\boldsymbol{q},\boldsymbol{t})\right|$ for the scattered electric field

During a typical dynamic light scattering measurement performed using the homodyne detection method,[51] the fluctuating scattered light intensity $I_s(\boldsymbol{q}, t)$ is recorded and used to construct the normalized intensity autocorrelation function

$$g^{(2)}(\boldsymbol{q}, t) = \frac{\langle I_s(\boldsymbol{q}, 0) I_s(\boldsymbol{q}, t)\rangle}{\langle {I_s}^2(\boldsymbol{q}, 0)\rangle} \ . \tag{17}$$

If the scattering volume V can be subdivided into regions that scatter light independently from one another, and if each subregion is big enough to hold a large number of particles, so that the central limit theorem applies and the scattered light intensity fluctuates as a Gaussian random variable, then the Siegert relation can be used to relate the normalized intensity autocorrelation function,[51]

$$g^{(2)}(\boldsymbol{q},t) = 1 + \left|g^{(1)}(\boldsymbol{q},t)\right|^2 \ , \tag{18}$$

to the normalized field autocorrelation function

$$g^{(1)}(\boldsymbol{q},t) = \frac{\langle E_s{}^*(\boldsymbol{q},0)E_s(\boldsymbol{q},t)\rangle}{\langle |E_s(\boldsymbol{q},0)|^2\rangle} \ , \tag{19}$$

where $E_s(\boldsymbol{q},t)$ is the magnitude of the scattered electric field. A theoretical result for $E_s(\boldsymbol{q},t)$ can be derived for linearly polarized, plane wave electromagnetic radiation that scatters from an isotropic liquid sample within the scattering[31, 32] volume V, into a detector located a distance R that is far from the scattering source. The far-field solution to Maxwell's equations in the Born approximation, which neglects phase shift contributions to $E_s(\boldsymbol{q},t)$ resulting from light traveling through particles with a different refractive index than that of the solvent, and with negligible variations in the polarization direction upon scattering, provides the following result for the magnitude of the scattered electric field at the detector[52]

$$E_s(\boldsymbol{q},t) = -\frac{{k_f}^2 E_0 V}{4\pi R\varepsilon_0} e^{i(k_f R-\omega_i t)}\delta\varepsilon(\boldsymbol{q},t) \, . \tag{20}$$

Here, E_0 is the magnitude of the incident electric field, k_f is the magnitude of the propagation vector of scattered light, ω_i is the incident light frequency, and $\delta\varepsilon(\boldsymbol{q},t)$ is a spatial Fourier transform of the local dielectric fluctuation (relative permittivity),

$$\delta\varepsilon(\boldsymbol{q},t) = \frac{1}{V}\int_V dr^3\, e^{i\boldsymbol{q}\cdot\boldsymbol{r}}\delta\varepsilon(\boldsymbol{r},t) \ , \tag{21}$$

where $\boldsymbol{r}$ is the position vector. Using eqn (20), the field autocorrelation function is related to fluctuations in the local dielectric constant via[52]

$$\langle E_s{}^*(\boldsymbol{q},0)E_s(\boldsymbol{q},t)\rangle = \frac{I_0 V^2 {k_f}^4}{16\pi^2 R^2 {\varepsilon_0}^2}\langle \delta\varepsilon^*(\boldsymbol{q},0)\delta\varepsilon(\boldsymbol{q},t)\rangle e^{-i\omega_i t} \ , \tag{22}$$

In eqn (22), $I_0 = {E_0}^2$ is the incident light intensity. For a non-magnetic, non-absorbing liquid, the dielectric constant is related to the solution refractive index via $n = \sqrt{\varepsilon}$. Furthermore, if the Dufour effect is negligible in a fluid with uniform temperature and pressure (satisfying $\delta T = \delta p = 0$ despite fluctuations in concentration), then the dielectric fluctuation $\delta\varepsilon(\boldsymbol{q},t)$ can be expanded using the chain rule at constant temperature and pressure,[21, 35, 42]

$$\delta\varepsilon(\boldsymbol{q},t) = 2n\sum_{i=1}^{2}\left(\frac{\partial n}{\partial \hat{C}_i}\right)_{p,T}\delta\hat{C}_i(\boldsymbol{q},t) \ . \tag{23}$$

According to the Onsager regression hypothesis,[1, 2] the mean regression of microscopic concentration fluctuations $\delta\hat{C}_i$ in eqn (23) decay by the same equations that govern the relaxation of macroscopic concentration fluctuations, which satisfy $\langle \delta\hat{C}_i{}^2\rangle \gg k_B T/\left(V\hat{G}_i\right)$. Hence, the diagonalized, Fourier transformed version of Fick's law in the limit $qR_{i^*} \to 0$ governs the relaxation of perpetually recurring microscopic fluctuations in concentration $\delta\hat{C}_i$ via[35, 53]

$$\frac{\partial\delta\hat{C}_i(\boldsymbol{q},t)}{\partial t} = -q^2\hat{D}_i\delta\hat{C}_i(\boldsymbol{q},t) + F_i(\boldsymbol{q},t) \ , \tag{24}$$

where $F_i(\boldsymbol{q},t)$ are random, fluctuating sources and $\hat{D}_i$ are elements of the diagonalized diffusivity matrix given by $[\hat{\mathbf{D}}] = [\mathbf{P}]^{-1}[\mathbf{D}][\mathbf{P}]$, and are equal to the eigenvalues of $[\mathbf{D}]$. The pair of Langevin equations, given by eqn (24), are solved to acquire the autocorrelation functions of the transformed concentration fluctuations in reciprocal space

$$\langle \delta\hat{C}_i{}^*(\boldsymbol{q},0)\delta\hat{C}_i(\boldsymbol{q},t)\rangle = \langle\left|\delta\hat{C}_i(\boldsymbol{q},0)\right|^2\rangle\, exp\left(-q^2\hat{D}_i t\right) \ . \tag{25}$$

Eqn (16), (19), (22), (23) and (25) combine to provide the absolute value of the normalized field autocorrelation function (see section 1.3 of SI)

$$\left|g^{(1)}(\boldsymbol{q},t)\right| = \left(\frac{B}{1+B}\right)exp(-q^2 D_- t) + \left(\frac{1}{1+B}\right)exp(-q^2 D_+ t) \ , \tag{26}$$

where the mode amplitude ratio B equals

$$B = \left(\frac{\hat{R}_a}{\hat{R}_s}\right)^2\left(\frac{\hat{G}_s}{\hat{G}_a}\right) \ . \tag{27}$$

Here, components 1 and 2 have been designated as the solute (a) and hydrated surfactant (s), respectively.

Eqn (26) indicates that concentration fluctuations in a ternary mixture at constant temperature and pressure decay via two mass diffusion relaxation modes, governed by the eigenvalues of the diffusivity matrix (*cf*. eqn (13) and (14)),

$$D_- = \frac{(D_{aa}+D_{ss})}{2} - \frac{\sqrt{(D_{aa}-D_{ss})^2 + 4D_{as}D_{sa}}}{2} \tag{28}$$

and

$$D_+ = \frac{(D_{aa}+D_{ss})}{2} + \frac{\sqrt{(D_{aa}-D_{ss})^2 + 4D_{as}D_{sa}}}{2} \ . \tag{29}$$

The eigenvalue diffusivities D_- and D_+ correspond to long-time diffusion, imposed by the limit $qR_{i^*} \to 0$, which indicates that the diffusion length scale, defined by q^{-1}, extends many particle radii.[54]

In eqn (27), the transformed refractive index derivatives $\hat{R}_i = \left(\partial n/\partial\hat{C}_i\right)_{p,T,\hat{C}_{j\neq i}}$ are

$$\hat{R}_a = P_{aa}R_a + P_{sa}R_s \tag{30}$$

and

$$\hat{R}_s = P_{as}R_a + P_{ss}R_s \ , \tag{31}$$

where the measurable refractive index increments $R_i = (\partial n/\partial C_i)_{p,T,C_{j\neq i}}$ are given by (see section 2.1 of SI)

$$R_a = \bar{V}_a\left(\frac{\partial n}{\partial \phi}\right)_{p,T,C_a/C_s} + \frac{1}{C_s}\left\{\frac{\partial n}{\partial (C_a/C_s)}\right\}_{p,T,\phi} \quad (32)$$

and

$$R_s = \bar{V}_{hs}\left(\frac{\partial n}{\partial \phi}\right)_{p,T,C_a/C_s} - \frac{\bar{V}_{hs}\, C_a/C_s}{(\phi-\phi_a)}\left\{\frac{\partial n}{\partial (C_a/C_s)}\right\}_{p,T,\phi} . \quad (33)$$

Here, $\bar{V}_{hs} = \bar{V}_s + n_H\bar{V}_w$ is the hydrated surfactant molar volume, ϕ is the micelle volume fraction, and $\phi_a = C_a\bar{V}_a$ is the solute volume fraction. The matrix $[\mathbf{P}]$ is given by eqn (12),

$$\begin{bmatrix} P_{aa} & P_{as} \\ P_{sa} & P_{ss} \end{bmatrix} = \begin{bmatrix} 1 & \left(\frac{D_{as}}{D_+ - D_{aa}}\right) \\ \left(\frac{D_- - D_{aa}}{D_{as}}\right) & 1 \end{bmatrix}, \quad (34)$$

and the elements of $[\hat{\mathbf{G}}]$ are determined using

$$\hat{G}_a = G_{aa}{P_{aa}}^2 + 2G_{as}P_{aa}P_{sa} + G_{ss}{P_{sa}}^2 \quad (35)$$

and

$$\hat{G}_s = G_{aa}{P_{as}}^2 + 2G_{as}P_{as}P_{ss} + G_{ss}{P_{ss}}^2 , \quad (36)$$

where G_{aa}, G_{as}, and G_{ss} are calculated via eqn (9) and P_{aa}, P_{as}, P_{sa}, and P_{ss} are given in eqn (34).

4.1.3 Rayleigh ratio

If the solution within the scattering volume is ergodic on the time scale of the measurement, then the time-averaged scattered light intensity recorded during a static light scattering (SLS) measurement is equal to the ensemble averaged static correlation function of the scattered electric field, which is given by eqn (22) with $t = 0$:

$$\langle I_s(\boldsymbol{q})\rangle = \langle |E_s(\boldsymbol{q},0)|^2\rangle = \frac{I_0V^2{k_f}^4}{16\pi^2R^2\varepsilon^2}\langle \delta\varepsilon^*(\boldsymbol{q},0)\delta\varepsilon(\boldsymbol{q},0)\rangle . \quad (37)$$

Combining eqn (16), (23), and (37), setting $\varepsilon^2 = n^4$ and $k_f \approx 2\pi n/\lambda_0$, where λ_0 is the wavelength of incident light, and taking the limit $qR_{i^*} \to 0$, one can write (see section 1.3 of SI)

$$\langle I_s(\boldsymbol{q})\rangle = \frac{I_0V}{R^2}\frac{4\pi^2n^2}{{\lambda_0}^4}{\hat{R}_s}^2\left(\frac{k_BT}{\hat{G}_s}\right)(1+B) . \quad (38)$$

The Rayleigh ratio is defined as $R_{90} = \langle I_s(\boldsymbol{q})\rangle R^2/(I_0V)$. Hence,

$$R_{90} = \frac{4\pi^2n^2}{{\lambda_0}^4}{\hat{R}_s}^2\left(\frac{k_BT}{\hat{G}_s}\right)(1+B) . \quad (39)$$

Evaluation of R_{90} thus requires knowledge of the chemical potential derivatives, refractive index increments, and the ternary diffusion coefficient matrix. The dependence of R_{90} on $[\mathbf{D}]$ may seem surprising, since R_{90} is an equilibrium function, and therefore should not depend on hydrodynamic parameters, such as the solvent viscosity or the bulk mobility coefficients, which characterize dissipation in a system undergoing an irreversible process. However, the relationship between R_{90} and $[\mathbf{D}]$ is a consequence of our choice for the matrix used to diagonalize $[\mathbf{G}]$, which is not unique, as discussed by Bardow.[21] Alternatively, we could have defined a modal matrix for $[\mathbf{G}]$, which is not constructed using transport coefficients. In general, the hydrodynamic parameters implied by eqn (39) are expected to cancel, a result that is shown in the sections that follow for all of the limiting special cases presented in this work (*cf.* eqn (93), (116), (132), (146), (147), and (166)).

4.2 Chemical potential derivatives for nonionic micellar solutions with hydrophobic solutes

Thermodynamic equilibrium relations for an n-component micellar solution with N different micelle types, comprised of solute (a), hydrated surfactant (s), and solvent (n), are given by (see section 2.2 of SI)

$$n_k\mu_a + m_k\mu_s = \mu_k \quad for\ k = 1,2,\dots,N . \quad (40)$$

In eqn (40), m_k is the micelle aggregation number for the micelle type k, n_k is the corresponding number of solutes per micelle, and μ_a, μ_s, and μ_k are chemical potentials for the solute, surfactant, and micelle species k, respectively, and are defined per eqn (10). Differentiation of eqn (40) with respect to either C_a or C_s at constant V, T and μ_n, followed by expansion of the micelle chemical potential derivatives using the chain rule, yields

$$n_k\left(\frac{\partial\mu_a}{\partial C_a}\right)_{T,\mu_n} + m_k\left(\frac{\partial\mu_s}{\partial C_a}\right)_{T,\mu_n} = \sum_{j=1}^{N}\left(\frac{\partial\mu_k}{\partial C_j}\right)_{T,\mu_n}\left(\frac{\partial C_j}{\partial C_a}\right) \quad (41)$$

and

$$n_k\left(\frac{\partial\mu_a}{\partial C_s}\right)_{T,\mu_n} + m_k\left(\frac{\partial\mu_s}{\partial C_s}\right)_{T,\mu_n} = \sum_{j=1}^{N}\left(\frac{\partial\mu_k}{\partial C_j}\right)_{T,\mu_n}\left(\frac{\partial C_j}{\partial C_s}\right) . \quad (42)$$

Here, contributions from free molecular solute and surfactant monomer to the thermodynamic derivatives, and thereby on the driving forces for the diffusion of solute and surfactant, have been neglected. We note that the summations in eqn (41) and (42) then index over N micelle species, rather than $n-1$ mixture components. In addition, we assume a 1:1 correspondence between the number of solute and surfactant molecules for each micelle type. Thus, $k = 1$ corresponds to the only solute-free micelle species considered in this model, comprised of $n_1 = 0$ solute molecules and m_1 surfactant monomers. Hence, for $k = 1$, eqn (41) and (42) become

$$m_1\left(\frac{\partial\mu_s}{\partial C_a}\right)_{T,\mu_n} = \sum_{j=1}^{N}\left(\frac{\partial\mu_1}{\partial C_j}\right)_{T,\mu_n}\left(\frac{\partial C_j}{\partial C_a}\right) \quad (43)$$

and

$$m_1\left(\frac{\partial\mu_s}{\partial C_s}\right)_{T,\mu_n} = \sum_{j=1}^{N}\left(\frac{\partial\mu_1}{\partial C_j}\right)_{T,\mu_n}\left(\frac{\partial C_j}{\partial C_s}\right) . \quad (44)$$

Furthermore, multiplication of eqn (41) and (42) by C_k and summation over all micelle types provides the result

$$C_a\left(\frac{\partial \mu_a}{\partial C_a}\right)_{T,\mu_n} + C_s\left(\frac{\partial \mu_s}{\partial C_a}\right)_{T,\mu_n} = \left(\frac{\partial \Pi}{\partial C_a}\right)_{T,\mu_n} \tag{45}$$

and

$$C_a\left(\frac{\partial \mu_a}{\partial C_s}\right)_{T,\mu_n} + C_s\left(\frac{\partial \mu_s}{\partial C_s}\right)_{T,\mu_n} = \left(\frac{\partial \Pi}{\partial C_s}\right)_{T,\mu_n}, \tag{46}$$

where the osmotic pressure derivatives at right are given by (see section 2.3 of SI)

$$\left(\frac{\partial \Pi}{\partial C_a}\right)_{T,\mu_n} = \sum_{k=1}^{N}\sum_{j=1}^{N} C_k\left(\frac{\partial \mu_k}{\partial C_j}\right)_{T,\mu_n}\left(\frac{\partial C_j}{\partial C_a}\right) \tag{47}$$

and

$$\left(\frac{\partial \Pi}{\partial C_s}\right)_{T,\mu_n} = \sum_{k=1}^{N}\sum_{j=1}^{N} C_k\left(\frac{\partial \mu_k}{\partial C_j}\right)_{T,\mu_n}\left(\frac{\partial C_j}{\partial C_s}\right). \tag{48}$$

The micelle chemical potential derivatives at constant T and μ_n are generally written as a sum of ideal and nonideal terms,[14, 39]

$$\frac{1}{N_A k_B T}\left(\frac{\partial \mu_k}{\partial C_j}\right)_{T,\mu_n} = \frac{\delta_{kj}}{C_k} + A_{kj}\,, \tag{49}$$

where the non-ideal mixing contribution A_{kj} captures the influence of interparticle interactions between micelles of various types. The following symmetry relation for $[\mathbf{G}]$ (see section 1.1 of SI)

$$\left(\frac{\partial \mu_a}{\partial C_s}\right)_{T,\mu_n} = \left(\frac{\partial \mu_s}{\partial C_a}\right)_{T,\mu_n}, \tag{50}$$

enforces equality between mixed partial derivatives of the total McMillan-Mayer free energy of the mixture with respect to solute and surfactant concentration.[55] Eqn (43)–(46), (49), and (50) combine to provide the elements $G_{ik} = (\partial \mu_i/\partial C_k)_{T,\mu_n}$ of the chemical potential derivative matrix $[\mathbf{G}]$

$$C_a G_{aa} = \left(\frac{\partial \Pi}{\partial C_a}\right)_{T,\mu_n} - C_s G_{sa}\,, \tag{51}$$

$$G_{as} = G_{sa} = \left(\frac{N_A k_B T}{m_1}\right)\left\{\frac{1}{C_a}\frac{\partial lnC_1}{\partial lnC_a} + \sum_{j=1}^{N} A_{1j}\left(\frac{\partial C_j}{\partial C_a}\right)\right\}, \tag{52}$$

and

$$C_s G_{ss} = \left(\frac{\partial \Pi}{\partial C_s}\right)_{T,\mu_n} - C_a G_{sa}\,. \tag{53}$$

Eqn (51)–(53) define chemical potential derivatives for polydisperse mixtures of spherical particles with arbitrary interaction potentials and concentrations. In eqn (52), the solute-free micelle concentration derivative $\partial lnC_1/\partial lnC_a$ accounts for variations in the solute-free micelle mixing entropy with respect to the local solute concentration C_a. For instance, as C_a increases, the micelle distribution shifts toward micelles that contain more solutes, causing C_1, and thereby the solute-free micelle mixing entropy, to decrease. In addition, A_{1j} captures the influence of inter-micellar interactions between solute-free and various type j micelles.

4.3 Ternary diffusion coefficient matrix $[\mathbf{D}]$ for nonionic micellar solutions with hydrophobic solutes

In order to determine the gradient diffusion coefficient matrix $[\mathbf{D}]$, and thereby the modal matrix $[\mathbf{P}]$, we briefly review a theoretical model introduced in our earlier work,[8, 9] which is based on Batchelor's[38-40] theory for gradient diffusion in polydisperse colloidal mixtures, to describe gradient diffusion in solute-containing micellar solutions with negligible molecular species. According to this theory, ternary mixtures of solute (a), surfactant (s), and solvent (n) are modelled as polydisperse, colloidal dispersions containing N different particle types, self-assembled from various numbers of solute and surfactant molecules. The molar diffusive flux $\boldsymbol{J}_i$ of a micelle species i containing n_i solutes and m_i surfactants, defined relative to a volume-fixed frame of reference at constant temperature and pressure is given by (see section 2.4 of SI)

$$\boldsymbol{J}_i = C_i \boldsymbol{v}_i$$
$$for\ i\ =\ 1,2,\ldots,N\ , \tag{54}$$

where $\boldsymbol{v}_i$ is the average diffusion velocity for the micelle species i. For small disturbances from equilibrium, the velocity $\boldsymbol{v}_i$ (and thereby the flux $\boldsymbol{J}_i$) is linearly related to the fundamental driving forces $\boldsymbol{X}_k$ for mass diffusion according to[39, 56]

$$\boldsymbol{v}_i = \frac{D_i^0}{N_A k_B T}\sum_{k=1}^{N} B_{ik}\boldsymbol{X}_k\ . \tag{55}$$

Here, D_i^0 is the infinite dilution diffusivity and B_{ik} is the bulk mobility coefficient, which relates the average velocity of a micelle species i to a steady thermodynamic driving force applied to a micelle species k, and accounts for the influence of multi-body hydrodynamic interactions on $\boldsymbol{v}_i$.

The diffusive fluxes $\boldsymbol{J}_i$ and corresponding driving forces $\boldsymbol{X}_k$ are linked by the reference frame in which they are defined, and are sometimes referred to as conjugates. For diffusion relative to a frame in which the flux of material volume is zero, the conjugate driving forces are given by (see section 2.4 of SI)

$$\boldsymbol{X}_k = -(\boldsymbol{\nabla}\mu_k)_{T,\mu_n}\ , \tag{56}$$

and the solvent is force-free according to

$$\boldsymbol{X}_n = -(\boldsymbol{\nabla}\mu_n)_{T,\mu_n} = 0\ . \tag{57}$$

Eqn (56) is expanded per the chain rule to yield

$$\boldsymbol{X}_k = -(\boldsymbol{\nabla}\mu_k)_{T,\mu_n} = -\sum_{j=1}^{N}\left(\frac{\partial \mu_k}{\partial C_j}\right)_{T,\mu_n}\boldsymbol{\nabla}C_j\ , \tag{58}$$

and the result is combined with eqn (1), (54), and (55) to produce the following $N \times N$ particle diffusion coefficient matrix

$$D_{ij} = \frac{D_i^0}{N_A k_B T} \sum_{k=1}^{N} B_{ik} C_i \left(\frac{\partial \mu_k}{\partial C_j}\right)_{T,\mu_n}$$
$$for\ i,j\ =\ 1,2,\ldots,N\ . \qquad (59)$$

In order to relate the matrix D_{ij} to the ternary diffusion coefficient matrix $[\mathbf{D}]$, the net flux of solute $\boldsymbol{J}_a$ and surfactant $\boldsymbol{J}_s$ are expressed using Fick's law and related to the micelle species fluxes $\boldsymbol{J}_i$ via weighted sums according to

$$\boldsymbol{J}_a = \sum_{i=1}^{N} n_i \boldsymbol{J}_i = -D_{aa}\boldsymbol{\nabla} C_a - D_{as}\boldsymbol{\nabla} C_s \qquad (60)$$

and

$$\boldsymbol{J}_s = \sum_{i=1}^{N} m_i \boldsymbol{J}_i = -D_{sa}\boldsymbol{\nabla} C_a - D_{ss}\boldsymbol{\nabla} C_s\ , \qquad (61)$$

where flux contributions from molecular solute and surfactant monomer have been neglected. The ternary diffusivity matrix $[\mathbf{D}]$ is then determined by expanding eqn (1) with the chain rule and combining the result with eqn (59)–(61) to produce

$$D_{aa} = \sum_{i=1}^{N}\sum_{j=1}^{N}\sum_{k=1}^{N} \frac{n_i D_i^0}{N_A k_B T} B_{ik} C_i \left(\frac{\partial \mu_k}{\partial C_j}\right)_{T,\mu_n} \frac{\partial C_j}{\partial C_a}\ , \qquad (62)$$

$$D_{as} = \sum_{i=1}^{N}\sum_{j=1}^{N}\sum_{k=1}^{N} \frac{n_i D_i^0}{N_A k_B T} B_{ik} C_i \left(\frac{\partial \mu_k}{\partial C_j}\right)_{T,\mu_n} \frac{\partial C_j}{\partial C_s}\ , \qquad (63)$$

$$D_{sa} = \sum_{i=1}^{N}\sum_{j=1}^{N}\sum_{k=1}^{N} \frac{m_i D_i^0}{N_A k_B T} B_{ik} C_i \left(\frac{\partial \mu_k}{\partial C_j}\right)_{T,\mu_n} \frac{\partial C_j}{\partial C_a}\ , \qquad (64)$$

and

$$D_{ss} = \sum_{i=1}^{N}\sum_{j=1}^{N}\sum_{k=1}^{N} \frac{m_i D_i^0}{N_A k_B T} B_{ik} C_i \left(\frac{\partial \mu_k}{\partial C_j}\right)_{T,\mu_n} \frac{\partial C_j}{\partial C_s}\ . \qquad (65)$$

Eqn (62)—(65) are valid for mixtures of polydisperse particles with arbitrary shapes, sizes, and concentrations, but are intractable in their present form. However, the result for $[\mathbf{D}]$ above can be simplified following Batchelor,[39] without loss of generality, by recasting the bulk mobility coefficient B_{ik} according to

$$B_{ik} = \delta_{ik}\left(1 + \sum_{l=1}^{N} f_{il}\phi_l\right) + g_{ik}\phi_k\ . \qquad (66)$$

Here, f_{il} and g_{ik} are unknown functions which may depend on solution properties such as the micelle species volume fractions, size and shape parameters, and the spatial distribution of the micelles. As discussed by Batchelor,[39] when $k = i$ the main terms B_{ii} of the bulk mobility coefficient matrix, given by

$$B_{ii} = 1 + (f_{ii} + g_{ii})\phi_i + \sum_{l\neq i}^{N} f_{il}\phi_l\ , \qquad (67)$$

express the influence of multi-body hydrodynamic interactions involving (1) identical particles of type i, each of which are under the influence of a steady thermodynamic driving force, where the contribution $(f_{ii} + g_{ii})\phi_i$ is identical to that of a monodisperse mixture of particles at volume fraction ϕ_i, and (2) hydrodynamic interactions involving i particles on which a force acts and force-free particles of type l, where the number of such cross coupling interactions is proportional to ϕ_l. When $k \neq i$, the off-diagonal coefficients $B_{ik,k\neq i}$ of the bulk mobility matrix are expressed via

$$B_{ik,k\neq i} = g_{ik}\phi_k\ . \qquad (68)$$

Here, the relevant interactions involve force-free i particles and k-type particles acted on by a force, where the number of such cross-coupling interactions is proportional to ϕ_k.

Using eqn (49), and (62)—(66), the matrix $[\mathbf{D}]$ can be re-written in the following more convenient form

$$D_{aa} = \sum_{i=1}^{N} n_i D_i^0 \left\{\left(1 + \sum_{k=1}^{N} f_{ik}\phi_k\right)\frac{\partial C_i}{\partial C_a} + \phi_i \sum_{j=1}^{N} h_{ij}\frac{\partial C_j}{\partial C_a}\right\}\ , \qquad (69)$$

$$D_{as} = \sum_{i=1}^{N} n_i D_i^0 \left\{\left(1 + \sum_{k=1}^{N} f_{ik}\phi_k\right)\frac{\partial C_i}{\partial C_s} + \phi_i \sum_{j=1}^{N} h_{ij}\frac{\partial C_j}{\partial C_s}\right\}\ , \qquad (70)$$

$$D_{sa} = \sum_{i=1}^{N} m_i D_i^0 \left\{\left(1 + \sum_{k=1}^{N} f_{ik}\phi_k\right)\frac{\partial C_i}{\partial C_a} + \phi_i \sum_{j=1}^{N} h_{ij}\frac{\partial C_j}{\partial C_a}\right\}\ , \qquad (71)$$

and

$$D_{ss} = \sum_{i=1}^{N} m_i D_i^0 \left\{\left(1 + \sum_{k=1}^{N} f_{ik}\phi_k\right)\frac{\partial C_i}{\partial C_s} + \phi_i \sum_{j=1}^{N} h_{ij}\frac{\partial C_j}{\partial C_s}\right\}\ , \qquad (72)$$

where

$$\frac{h_{ij}}{\lambda_{ij}^{\ 3}} = \tilde{A}_{ij} + g_{ij} + \sum_{k=1}^{N}\left(\tilde{A}_{ij}f_{ik} + g_{ik}\tilde{A}_{kj}\right)\phi_k\ . \qquad (73)$$

Here, $\tilde{A}_{kj} = A_{kj}/\overline{V}_j$ is a dimensionless function that captures the influence of thermodynamic interparticle interactions between micelles of various types and $\lambda_{ij} = \left(V_j/V_i\right)^{1/3}$ is a size ratio where V_i and V_j are the volumes of a type i and j micelle, respectively. Rigorous theoretical results for the hydrodynamic functions f_{il}, g_{ik}, and thereby h_{ij}, applicable to concentrated dispersions, are currently unavailable. However, as shown in the sections that follow, we will not need to define them to derive analytical expressions for the scattering functions at arbitrary concentration in the limit of zero local polydispersity.

4.4 $[\mathbf{D}]$, $[\mathbf{P}]$, $\left|\boldsymbol{g}^{(1)}(\boldsymbol{q},\boldsymbol{t})\right|$, and $\boldsymbol{R_{90}}$ for locally monodisperse, nonionic micellar solutions with hydrophobic solutes

We now examine the scattering functions described by eqn (26) and (39) for the special case in which local micelle polydispersity is neglected. In this scenario, the micelle distribution is modelled using a Kronecker delta function with a composition dependent mean

$$C_i = \frac{C_s}{\bar{m}}\delta_{ii^*} = \begin{Bmatrix} \frac{C_s}{\bar{m}} \; when \; i = i^* \\ 0 \; when \; i \neq i^* \end{Bmatrix} \; , \tag{74}$$

where i^* designates a micelle type with $\bar{n}$ solutes, $\bar{m}$ surfactants, radius R_{i^*}, and a local concentration equal to $C_s/\bar{m}$. Such a delta distribution is consistent with thermodynamic theory for self-assembly of surfactant and hydrophobic solutes.[57] Using eqn (69)–(74), the corresponding ternary diffusion coefficient matrix $[\mathbf{D}]$ for locally monodisperse micellar solutions comprising nonionic surfactants and hydrophobic solutes was determined to be (see section 2.5.1 in SI)

$$\frac{D_{aa}}{D_{i^*}^0} = 1 + f\phi - \mathcal{M} \; , \tag{75}$$

$$\frac{D_{as}}{D_{i^*}^0} = \frac{C_a}{C_s}(h\phi + L\phi^2 + \mathcal{M}) \; , \tag{76}$$

$$\frac{D_{sa}}{D_{i^*}^0} = -\frac{C_s}{C_a}\mathcal{M} \; , \tag{77}$$

and

$$\frac{D_{ss}}{D_{i^*}^0} = 1 + (f + h)\phi + L\phi^2 + \mathcal{M} \, , \tag{78}$$

where the functions $\mathcal{M}$, h , L, and L_a are given by

$$\mathcal{M} = \frac{\partial lnR_{i^*}}{\partial lnC_a}[1 + (f + 3h)\phi] - h\phi_a - C_a L_a \phi \, , \tag{79}$$

$$h = \tilde{A} + g + (f + g)\tilde{A}\phi \; , \tag{80}$$

$$L = \frac{\partial f}{\partial \phi} + \left[\frac{\partial (h_{ii^*} - f_{ii^*})}{\partial \phi}\right]_{i=i^*} - \left(\frac{\partial h_{ij}}{\partial \phi}\right)_{j=i=i^*} \; , \tag{81}$$

and

$$L_a = \frac{\partial f}{\partial C_a} + \left[\frac{\partial (h_{ii^*} - f_{ii^*})}{\partial C_a}\right]_{i=i^*} - \left(\frac{\partial h_{ij}}{\partial C_a}\right)_{j=i=i^*} \; . \tag{82}$$

Here, $\tilde{A}$, f, and g are functions that account for multi-body interactions between identical micelles of the same species, and the function $\mathcal{M}$ captures the influence of variations in the average micelle size and aggregation number along gradients in solute or surfactant concentration.

Using eqn (28), (29), and (75)–(78), the corresponding eigenvalues of $[\mathbf{D}]$ are given by

$$\frac{D_-}{D_{i^*}^0} = 1 + f\phi \tag{83}$$

and

$$\frac{D_+}{D_{i^*}^0} = 1 + (f + h)\phi + L\phi^2 \; . \tag{84}$$

indicating that the $(-)$ and $(+)$ eigenmodes for diffusion correspond to long-time self and gradient diffusion coefficients for monodisperse, rigid particles, respectively (see section 2.5.2 of SI). We note that this result is exact and supports arguments by Pusey for bimodal decay of the field correlation function, corresponding to self and gradient diffusion in narrowly polydisperse particle dispersions.[15] Eqn (34), (75)–(78), (83) and (84) combine to produce the following modal matrix for $[\mathbf{D}]$,

$$[\mathbf{P}] = \begin{bmatrix} P_{aa} & P_{as} \\ P_{sa} & P_{ss} \end{bmatrix} = \begin{bmatrix} 1 & C_a/C_s \\ \frac{C_s/C_a\mathcal{M}}{h\phi + L\phi^2 + \mathcal{M}} & 1 \end{bmatrix} \; . \tag{85}$$

In order to determine the elements of the matrix $[\boldsymbol{G}]$ in the limit of zero local polydispersity, we start by evaluating the solute-free micelle concentration derivative $\partial lnC_1/\partial lnC_a$, shown in eqn (52). Consider a Gaussian micelle distribution function given by

$$C_i = \frac{C_s}{\bar{m}} \frac{exp\left\{-\frac{1}{2}\left(\frac{n_i - \bar{n}}{\sigma}\right)^2\right\}}{\sigma\sqrt{2\pi}}, \tag{86}$$

where σ^2 is the distribution variance. Differentiating eqn (86) with respect to solute concentration C_a for $i = 1$ yields

$$\frac{\partial lnC_1}{\partial lnC_a} = -\left(\frac{\bar{n}}{\sigma}\right)^2 \left(1 + \frac{\partial ln\bar{m}}{\partial lnC_a}\right) + \frac{\partial lnC_{tot}}{\partial lnC_a}, \tag{87}$$

where we have used $\bar{n} = \bar{m}\, C_a/C_s$ and $C_{tot} = C_s/\bar{m}$ is the total micelle concentration. In the limit as the variance approaches zero, eqn (86) becomes

$$\lim_{\sigma^2 \to 0} \frac{C_s}{\bar{m}} \frac{exp\left\{-\frac{1}{2}\left(\frac{n_i - \bar{n}}{\sigma}\right)^2\right\}}{\sigma\sqrt{2\pi}} = \frac{C_s}{\bar{m}}\delta_{ii^*}, \tag{88}$$

and eqn (87) yields

$$\lim_{\sigma^2 \to 0} \frac{\partial lnC_1}{\partial lnC_a} \to -\infty \; . \tag{89}$$

Hence, per eqn (52) and (89),

$$\lim_{\sigma^2 \to 0} G_{sa} \to -\infty \, , \tag{90}$$

and, per eqn (51)–(53) and (90), the elements $[\mathbf{G}]$ are infinite, except in special limiting cases. However, as shown in section 3.1 of SI, the scattering functions in this limit are finite.

Using eqn (26)–(36), (51)–(53), (84), and (85) one may determine the mode amplitude ratio (see section 3.1 of SI),

$$B = 0 \, , \tag{91}$$

and thereby the field correlation function

$$\left|g^{(1)}(\boldsymbol{q}, t)\right| = exp\{-q^2 D_{i^*}^0[1 + (f + h)\phi + L\phi^2]t\} \; , \tag{92}$$

which indicates monomodal decay via gradient diffusion. In addition, the Rayleigh ratio is determined to be (see section 3.1 of SI)

$$R_{90} = \frac{4\pi^2 n^2}{{\lambda_0}^4}\left(\frac{\partial n}{\partial \phi}\right)^2_{p,T,C_a/C_s} V_{i^*}\phi \left\{\frac{d[\phi Z(\phi)]}{d\phi}\right\}^{-1} \; , \tag{93}$$

where V_{i^*} is the volume of a type i^* micelle and $Z(\phi)$ is the compressibility factor. For monodisperse hard spheres, the latter is given accurately by the Carnahan–Starling equation[58]

$$Z(\phi) = \frac{\Pi}{C_{tot} N_A k_B T} = \frac{1 + \phi + \phi^2 - \phi^3}{(1-\phi)^3} \quad . \tag{94}$$

Remarkably, eqn (92) and (93) correspond to theoretical predictions for binary mixtures of monodisperse colloidal particles. These results indicate that multicomponent diffusion effects, such as uphill diffusion ($D_{sa} < 0$), which strongly affect the diffusivity matrix $[\mathbf{D}]$ per eqn (75)–(78) via the function $\mathcal{M}$, have no effect on the scattering functions $\left|g^{(1)}(q,t)\right|$ and R_{90} in the limit of negligible local polydispersity. These results provide theoretical support for earlier investigations by others,[12, 13, 46] who have used eqn (92)–(93) without *a priori* justification, to successfully model light scattering data from $C_{12}E_5$/decane/water solutions.

Finally, the Onsager coefficient matrix $[\mathbf{L}]$ is related to $[\mathbf{D}]$ and $[\mathbf{G}]$ via $[\mathbf{D}] = [\mathbf{L}][\mathbf{G}]$. Hence, the matrix $[\mathbf{G}]$ can be inverted to yield expressions for the Onsager coefficients

$$L_{aa} = (D_{aa}G_{ss} - D_{as}G_{sa})/|\boldsymbol{G}| \ , \tag{95}$$

$$L_{as} = (D_{as}G_{aa} - D_{aa}G_{as})/|\mathbf{G}| \ , \tag{96}$$

$$L_{sa} = (D_{sa}G_{ss} - D_{ss}G_{sa})/|\mathbf{G}| \ , \tag{97}$$

and

$$L_{ss} = (D_{ss}G_{aa} - D_{sa}G_{as})/|\mathbf{G}| \ , \tag{98}$$

where $|\mathbf{G}|$ is the determinant of the chemical potential derivative matrix $[\mathbf{G}]$**.** Using eqn (51)–(53), (75)–(78), and (95)–(98), one can derive the Onsager coefficients for concentrated mixtures of nonionic micelles with hydrophobic solutes (see section 3.2 of SI) to find

$$L_{aa} = \bar{n}^2 C_{tot} \left(\frac{D_{i^*}^0}{N_A k_B T}\right) K(\phi) \ , \tag{99}$$

$$L_{as} = L_{sa} = \bar{n}\bar{m} C_{tot} \left(\frac{D_{i^*}^0}{N_A k_B T}\right) K(\phi) \ , \tag{100}$$

and

$$L_{ss} = \bar{m}^2 C_{tot} \left(\frac{D_{i^*}^0}{N_A k_B T}\right) K(\phi) \ , \tag{101}$$

where $K(\phi)$ is a concentration dependent bulk mobility coefficient for dispersions of monodisperse particles.

Per eqn (100), the Onsager reciprocal relations are satisfied. Furthermore, the determinant $|\mathbf{L}| = L_{aa}L_{ss} - L_{as}L_{sa} = 0$, which indicates that the Onsager matrix $[\mathbf{L}]$ is singular, and thus not invertible, in the locally monodisperse limit as the micelle distribution variance approaches zero ($\sigma^2 \to 0$). This result is consistent with the $[\mathbf{G}]$ matrix given by eqn (51)–(53), whose elements approach infinity in this limit.

4.5 Scattering functions and transport coefficients for limiting special cases

In the following sections 4.5.1–3, we derive scattering functions and transport coefficients applicable to locally monodisperse micellar solutions that are either dilute, infinitely dilute, or at arbitrary concentration with trace amounts of solute. In section 4.5.4, the locally monodisperse assumption is relaxed, and the influence of optical polydispersity is explored in the label limit.

4.5.1 $[\mathbf{D}]$, $\left|\boldsymbol{g}^{(1)}(\boldsymbol{q},\boldsymbol{t})\right|$, and $\boldsymbol{R_{90}}$ for dilute mixtures ($\boldsymbol{\phi \ll 1}$)

For dilute mixtures that satisfy $\phi \ll 1$, where only interactions involving pairs of micelles are relevant, the functions $\tilde{A}_{kj}$, f_{il}, and g_{ik} reduce to the following, in agreement with theory by Batchelor,[38-40]

$$\tilde{A}_{kj} = \beta_{kj}\left(\frac{1+\lambda_{kj}}{2\lambda_{kj}}\right)^3 \ , \tag{102}$$

$$f_{il} = K'_{il} \ , \tag{103}$$

$$g_{ik} = K''_{ik} \ , \tag{104}$$

and

$$h_{ij} = \beta_{ij}\left(\frac{1+\lambda_{ij}}{2}\right)^3 + K''_{ij} \ . \tag{105}$$

Here, β_{kj} are 2nd osmotic virial coefficients, and K'_{il} and K''_{ik} are bulk mobility coefficients that characterise pairwise interactions between particles of various types. For dilute mixtures of interacting, polydisperse hard spheres, theoretical results for the virial coefficients are given by $\beta_{kj} = 8$.[59] In addition, estimates for the bulk mobility coefficients are provided by Batchelor[40] according to $K'_{il} = -2.5/(1 + 0.16\lambda_{il})$ and $K''_{ik} = {\lambda_{ik}}^2/\left(1 + {\lambda_{ik}}^2\right) - \left({\lambda_{ik}}^2 + 3\lambda_{ik} + 1\right)$, which yield results that are accurate to within 5% of numerical calculations over $1/8 \le \lambda_{ij} \le 8$.

Consistent with our previous work,[9] the ternary diffusion coefficient matrix $[\mathbf{D}]$ for dilute, locally monodisperse micellar solutions comprising nonionic surfactants and hydrophobic solutes can be determined using eqn (75)–(78) and (102)–(105) to yield

$$\frac{D_{aa}}{D_{i^*}^0} = 1 + K'\phi - M\left(\phi, \frac{C_a}{C_s}\right) \ , \tag{106}$$

$$\frac{D_{as}}{D_{i^*}^0} = \frac{C_a}{C_s}\left\{(\beta + K'')\phi + M\left(\phi, \frac{C_a}{C_s}\right)\right\} \ , \tag{107}$$

$$\frac{D_{sa}}{D_{i^*}^0} = -\frac{C_s}{C_a} M\left(\phi, \frac{C_a}{C_s}\right) \ , \tag{108}$$

and

$$\frac{D_{ss}}{D_{i^*}^0} = 1 + (\beta + S)\phi + M\left(\phi, \frac{C_a}{C_s}\right) , \tag{109}$$

where the function $M(\phi, C_a/C_s)$ is given by

$$M\left(\phi,\frac{C_a}{C_s}\right)=\frac{\partial lnR_{i^*}}{\partial lnC_a}(1+\chi\phi)-(\beta+K'')\phi_a \tag{110}$$

and the parameter χ is evaluated according to

$$\chi=\left(\frac{3}{2}\beta+K'+3K''\right)-\left\{\frac{d(K''-K')}{d\lambda}\right\}_{\lambda=1} . \tag{111}$$

Here, β is the 2nd osmotic virial coefficient, and K', K'', and $S=K'+K''$ are bulk mobility coefficients for dilute, monodisperse particle suspensions.

The corresponding eigenvalues of $[\mathbf{D}]$ are given by

$$\frac{D_-}{D_{i^*}^0}=1+K'\phi \tag{112}$$

and

$$\frac{D_+}{D_{i^*}^0}=1+(\beta+S)\phi \ . \tag{113}$$

Eqn (34), (106)–(109), (112) and (113) combine to produce the following modal matrix for $[\mathbf{D}]$,

$$[\mathbf{P}]=\begin{bmatrix}P_{aa} & P_{as}\\ P_{sa} & P_{ss}\end{bmatrix}=\begin{bmatrix}1 & C_a/C_s\\ \dfrac{C_s/C_aM(\phi,C_a/C_s)}{(\beta+K'')\phi+M(\phi,C_a/C_s)} & 1\end{bmatrix} . \tag{114}$$

Using eqn (92) and (103)–(105), the field autocorrelation function for dilute, locally monodisperse mixtures reduces to

$$\left|g^{(1)}(\boldsymbol{q},t)\right|=exp\{-q^2D_{i^*}^0[1+(\beta+S)\phi]t\} , \tag{115}$$

and the Rayleigh ratio is determined to be

$$R_{90}=\frac{4\pi^2n^2}{{\lambda_0}^4}\left(\frac{\partial n}{\partial\phi}\right)^2_{p,T,C_a/C_s}V_{i^*}\phi(1-\beta\phi), \tag{116}$$

4.5.2 $[\mathbf{D}]$, $\left|g^{(1)}(\boldsymbol{q},t)\right|$ and R_{90} at infinite dilution $\phi\to 0$

In the limit of infinite dilution ($\phi\to 0$), the diffusivity matrix $[\mathbf{D}]$ for locally monodisperse micellar solutions, given by eqn (75)–(78), reduces to

$$\frac{D_{\mathrm{aa}}}{D_{i^*}^0}=1-\frac{\partial lnR_{i^*}}{\partial lnC_a} , \tag{117}$$

$$\frac{D_{\mathrm{as}}}{D_{i^*}^0}=\frac{C_a}{C_s}\frac{\partial lnR_{i^*}}{\partial lnC_a} , \tag{118}$$

$$\frac{D_{\mathrm{sa}}}{D_{i^*}^0}=-\frac{C_s}{C_a}\frac{\partial lnR_{i^*}}{\partial lnC_a} , \tag{119}$$

and

$$\frac{D_{\mathrm{ss}}}{D_{i^*}^0}=1+\frac{\partial lnR_{i^*}}{\partial lnC_a} . \tag{120}$$

Per eqn (83) and (84), the corresponding eigenvalues become identical and equal to the Stokes-Einstein diffusivity

$$D_-=D_+=D_{i^*}^0 . \tag{121}$$

Eqn (26) and (121) combine to yield the expected result for the field correlation function at infinite dilution

$$\left|g^{(1)}(\boldsymbol{q},t)\right|=exp\left(-q^2D_{i^*}^0t\right) , \tag{122}$$

which indicates monomodal decay according to the solute-containing micelle Stokes-Einstein diffusivity. Furthermore, using eqn (93) with the relation $\phi=V_{i^*}c_s(N_A/MW_s)$ in the limit as $\phi\to 0$, for which $Z(\phi)\to 1$, one finds

$$\frac{K_sc_s}{R_{90}}=\frac{1}{MW_s} , \tag{123}$$

where c_s is the surfactant mass concentration, MW_s is the molecular weight of surfactant per micelle, N_A is Avogadro's number, and $K_s=4\pi^2n^2/\left(N_A{\lambda_0}^4\right)(\partial n/\partial c_s)^2_{p,T,C_a/C_s}$ is the optical contrast constant. The results given by eqn (122) and (123) indicate that micelle growth effects, which are responsible for significant multicomponent diffusion effects even as $\phi\to 0$ per eqn (117)–(120), do not affect the scattering functions at infinite dilution, enabling one to acquire estimates for average morphological parameters for solute-containing micelles, such as hydrodynamic radii R_{i^*} and aggregations numbers $\bar{m}$ with respect to composition C_a/C_s.

4.5.3 Tracer limit $C_a\to 0$ for $[\mathbf{G}]$, $\left|g^{(1)}(\boldsymbol{q},t)\right|$, and R_{90}

In this section, we evaluate the scattering functions and the chemical potential derivative matrix for the special case in which solute is present in vanishingly small amounts, corresponding to the tracer limit, $C_a\to 0$. In this scenario, the derivative G_{sa} , given by eqn (52), is finite. Hence, the matrix $[\mathbf{G}]$ can be evaluated given expressions for the osmotic pressure and the micelle chemical potential derivatives. Here, we use theoretical results by Vrij[17, 18] for polydisperse hard sphere mixtures in the Percus-Yevick approximation for the osmotic pressure

$$\frac{\Pi}{N_Ak_BT}=\frac{6}{\pi}\left\{\frac{\xi_0}{(1-\xi_3)}+\frac{3\xi_1\xi_2}{(1-\xi_3)^2}+\frac{3{\xi_2}^3}{(1-\xi_3)^3}\right\} \tag{124}$$

and the particle chemical potential derivatives

$$\begin{aligned}\frac{1}{N_Ak_BT}\left(\frac{\partial\mu_k}{\partial C_j}\right)_{T,\mu_n}=&\frac{\delta_{kj}}{C_k}\\&+\frac{\pi/6}{(1-\phi)}\{{d_k}^3+{d_j}^3+{d_k}^3{d_j}^3\eta_0\\&+3d_kd_j[d_k(1+d_k\eta_2)(1+{d_j}^2\eta_1)\\&+d_j(1+d_j\eta_2)(1+{d_k}^2\eta_1)]\\&+9{d_k}^2{d_j}^2\eta_2(1+d_k\eta_2)(1+d_j\eta_2)\}\end{aligned} \tag{125}$$

where d_k is the diameter of a type k particle,

$$\eta_\nu=\frac{\xi_\nu}{1-\phi} , \tag{126}$$

and

$$\xi_\nu=\frac{\pi}{6}\sum_{i=1}^{N}\frac{\phi_i}{V_i}{d_i}^\nu=\sum_{i=1}^{N}\phi_i\,{d_i}^{\nu-3} . \tag{127}$$

Using eqn (51)–(53) and (124)–(127), the chemical potential derivatives $[\mathbf{G}]$ for locally monodisperse micelles in the tracer limit are given by (see section 3.3 of SI)

$$\frac{C_a G_{aa}}{N_A k_B T} = 1 \ , \tag{128}$$

$$\frac{C_s G_{as}}{N_A k_B T} = \frac{C_s G_{sa}}{N_A k_B T} = -1 - \frac{3a_1}{m_1 R_1}\frac{(1+\phi+\phi^2)}{(1-\phi)^3} + \frac{V_a}{m_1 V_{hs}}\frac{(1+2\phi)^2}{(1-\phi)^4} \ , \tag{129}$$

and

$$\frac{C_s G_{ss}}{N_A k_B T} = \frac{1}{m_1}\frac{(1+2\phi)^2}{(1-\phi)^4} \ . \tag{130}$$

Here, a_1 is the micelle growth rate, which indicates how strongly the average micelle radius varies with the solute to surfactant molar ratio C_a/C_s, V_a is the molecular volume of the solute, and $V_{hs} = V_s + n_H V_w$ is the molecular volume of a hydrated surfactant monomer, where n_H is the hydration index, and V_w and V_s are the molecular volumes for the solvent and a dry surfactant molecule, respectively. Per eqn (128), when only trace amounts of solute are present, the chemical potential of the solute varies with respect to solute concentration via ideal mixing within the micellar solution. Eqn (130), on the other hand, describes variations in the surfactant chemical potential with respect to surfactant concentration resulting from the non-ideal mixing of interacting, monodisperse, solute-free micelles. Interestingly, the cross terms, given by eqn (129), describe variations in chemical potential that are affected by a term proportional to the micelle growth rate a_1 and the molecular volume of the solute V_a. These non-ideal contributions capture the influence of self-assembly on micellar solution thermodynamics and are not included in thermodynamic models derived for rigid particle dispersions.

In order to view the relative importance of the micellar growth contributions on the cross terms of the $[\mathbf{G}]$ matrix, theoretical predictions for $[\mathbf{G}]$ in the tracer limit for aqueous $C_{12}E_{10}$/decane mixtures were calculated using eqn (128)–(130) with $V_a = 0.32$ nm³, $V_s = 0.99$ nm³, $V_w = 0.03$ nm³, $m_1 = 103$, $n_H = 40$, $a_1 = 2.4226$ nm, and $R_1 = 3.76$ nm, consistent with our light scattering data shown in Fig. 3. The results are plotted versus volume fraction ϕ in Fig. 4. As shown, the main solute chemical potential derivative G_{aa} is independent of volume fraction, indicating that trace amounts of solute mix ideally within micelles, even in crowded mixtures. In contrast, the surfactant main term G_{ss} increases strongly with increasing volume fraction, resulting from the interactions between monodisperse solute-free micelles. Interestingly, the cross terms G_{as} and G_{sa} are shown to become more negative with increasing volume fraction, illustrating the influence of micelle growth effects on the matrix $[\mathbf{G}]$.

The tracer limit described in this section is a special case of the locally monodisperse limit discussed in section 4.4. Hence,

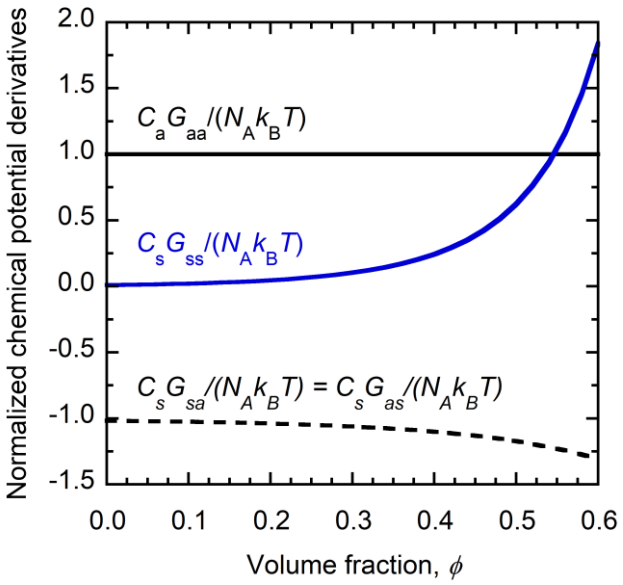

Fig. 4 Theoretical predictions for the normalized chemical potential derivatives $[\mathbf{G}]$, calculated using eqn (128)–(130) and plotted with respect to volume fraction for aqueous $C_{12}E_{10}$(s) + decane (a) in the tracer limit as $C_a \to 0$.

the scattering functions are determined via eqn (92) and (93) in the limit as $C_a \to 0$, to yield the field correlation function

$$\left|g^{(1)}(\boldsymbol{q},t)\right| = exp\{-q^2 D^0[1+(f+h)\phi+L\phi^2]t\} \ , \tag{131}$$

and the Rayleigh ratio

$$R_{90} = \frac{4\pi^2 n^2}{{\lambda_0}^4}\left(\frac{\partial n}{\partial \phi}\right)^2_{p,T,C_a/C_s} V_1 \phi \left\{\frac{d[\phi Z(\phi)]}{d\phi}\right\}^{-1} , \tag{132}$$

which are not restricted to the Percus-Yevick result for interacting hard spheres.

4.5.4 Label limit for $[\mathbf{D}]$, $[\mathbf{G}]$, $[\mathbf{L}]$, $\left|\boldsymbol{g}^{(1)}(\boldsymbol{q},\boldsymbol{t})\right|$, and $\boldsymbol{R_{90}}$

We now examine the transport coefficients and scattering functions described by eqn (26) and (39) for the special case in which the solute behaves as a volume-less label. In this scenario, solute-containing micelles are uniformly sized, but optically polydisperse, and the interactions between the various label-containing micelle species are identical. Hence, the ternary diffusion coefficient matrix $[\mathbf{D}]$ for the label case can be determined by setting $\lambda_{ij} = 1$, $\tilde{A}_{ij} = \tilde{A}$, $f_{ik} = f$, $g_{ik} = g$, and $h_{ij} = h$, so that eqn (69)–(72) simplify to

$$\frac{D_{aa}}{D^0} = 1 + f\phi \ , \tag{133}$$

$$\frac{D_{as}}{D^0} = \frac{C_a}{C_s}(h\phi + L\phi^2) \ , \tag{134}$$

$$D_{sa} = 0 \ , \tag{135}$$

and

$$\frac{D_{ss}}{D^0} = 1 + (f+h)\phi + L\phi^2 \ . \tag{136}$$

The corresponding eigenvalues of $[\mathbf{D}]$ are given by

$$\frac{D_-}{D^0} = 1 + f\phi \tag{137}$$

and

$$\frac{D_+}{D^0} = 1 + (f + h)\phi + L\phi^2 \ . \tag{138}$$

Using eqn (49), (51)–(53), (124), and (127), the solute and surfactant chemical potential derivatives reduce to (see section 3.4 of SI)

$$G_{aa} = -\frac{N_A k_B T}{\bar{n} C_a}\frac{\partial lnC_1}{\partial lnC_a} \ , \tag{139}$$

$$G_{as} = G_{sa} = \frac{N_A k_B T}{\bar{n} C_s}\frac{\partial lnC_1}{\partial lnC_a} \ , \tag{140}$$

and

$$G_{ss} = \frac{N_A k_B T}{m_1 C_s}\left\{\frac{d[\phi Z(\phi)]}{d\phi} - \frac{\partial lnC_1}{\partial lnC_a}\right\} \ . \tag{141}$$

where C_1 is the solute-free micelle concentration. Note, in this development it was not necessary to specify a particular micelle distribution function C_i, and, unlike our results presented in sections 4.4 and 4.5.3 for locally monodisperse micelles or in the tracer limit, respectively, the derivatives $\partial lnC_1/\partial lnC_a$ for the label limit are finite.

Furthermore, the Onsager matrix for the label limit is acquired using eqn (95)–(98), (133)–(136) and (139)–(141) (see section 3.4 of SI)

$$L_{aa} = \bar{n}^2 C_{tot}\left(\frac{D^0}{N_A k_B T}\right)\left[K(\phi) + \frac{1 + f\phi}{(-\partial lnC_1/\partial lnC_a)}\right] \ , \tag{142}$$

$$L_{as} = L_{sa} = \bar{n} m_1 C_{tot}\left(\frac{D^0}{N_A k_B T}\right)K(\phi) \ , \tag{143}$$

and

$$L_{ss} = {m_1}^2 C_{tot}\left(\frac{D^0}{N_A k_B T}\right)K(\phi) \ . \tag{144}$$

Per eqn (142), the main Onsager coefficient L_{aa}, which is related to the mobility of the solute when it is acted on a by a steady thermodynamic driving force, depends on the micelle distribution function through the derivative $\partial lnC_1/\partial lnC_a$, and, per eqn (143), the Onsager reciprocal relations are satisfied. In the limit of zero local polydispersity, the derivative $-\partial lnC_0/\partial lnC_a \to \infty$ and eqn (142)–(144) are shown to be consistent with eqn (99)–(101).

In order to determine the scattering functions, eqn (34) and (133)–(138) combine to produce the modal matrix for the label case,

$$[\mathbf{P}] = \begin{bmatrix} 1 & C_a/C_s \\ 0 & 1 \end{bmatrix} \ . \tag{145}$$

Eqn (27), (30)–(33), (39), (139)–(141), and (145), are then used to determine the Rayleigh ratio for the label limit (see section 3.4 of SI):

$$R_{90} = \frac{4\pi^2 n^2}{{\lambda_0}^4}\left(\frac{\partial n}{\partial \phi}\right)^2_{p,T,C_a/C_s} V_1\phi\left\{\frac{d[\phi Z(\phi)]}{d\phi}\right\}^{-1}(1 + B_{LL}) \ , \tag{146}$$

where the mode amplitude ratio B_{LL} for the label limit is given by

$$B_{LL} = \left\{\frac{[\partial n/\partial(C_a/C_s)]_{p,T,\phi}}{\phi(\partial n/\partial\phi)_{p,T,C_a/C_s}}\right\}^2 \frac{(C_a/C_s)^2}{(-\partial lnC_1/\partial lnC_a)}\frac{d[\phi Z(\phi)]}{d\phi}. \tag{147}$$

Per eqn (147), B_{LL} is generally nonzero. Hence, decay of the field correlation function, given by

$$\left|g^{(1)}(\boldsymbol{q}, t)\right| = \left(\frac{B_{LL}}{1 + B_{LL}}\right)exp(-q^2 D_- t) + \left(\frac{1}{1 + B_{LL}}\right)exp(-q^2 D_+ t) \ , \tag{148}$$

is bimodal, corresponding to the eigenvalue diffusivities given by eqn (137) and (138).

Theoretical predictions for $[\mathbf{G}]$ in the label limit for aqueous mixtures of label-containing $C_{12}E_{10}$ micelles were calculated using eqn (139)–(141) with $V_a = 0$ nm³, $V_s = 0.99$ nm³, $V_w = 0.03$ nm³, $m_1 = 103$, and $n_H = 40$, consistent with Fig. 3, with $C_a/C_s = 0.2$. To compare our calculations for $[\mathbf{G}]$ in the label limit with those shown in Figure 4 for the tracer limit, the Percus-Yevick result for compressibility factor $Z(\phi)$, applicable to monodisperse hard spheres,

$$Z(\phi) = \frac{\Pi}{C_{tot} N_A k_B T} = \frac{1 + \phi + \phi^2}{(1 - \phi)^3} \ , \tag{149}$$

was used to calculate the derivative $d[\phi Z(\phi)]/d\phi$. In addition,

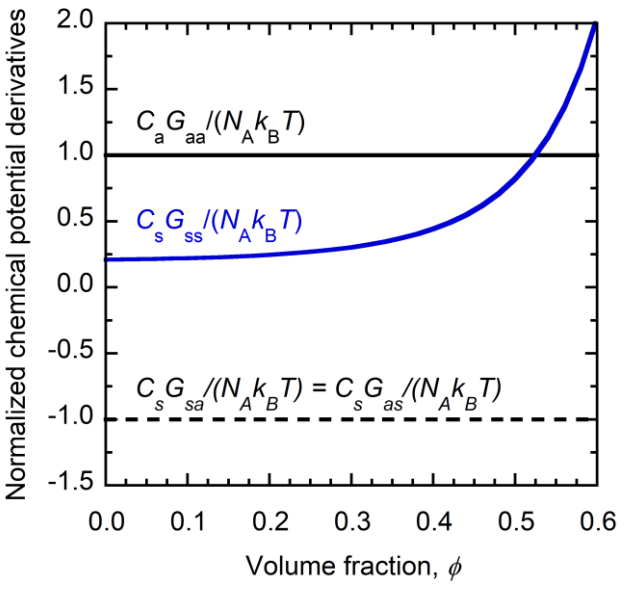

Fig. 5 Theoretical predictions in the label limit for the normalized chemical potential derivatives $[\mathbf{G}]$, calculated using eqn (139)–(141) and (149) and plotted with respect to volume fraction for aqueous $C_{12}E_{10}$ (s) micelles with Poisson distributed solute labels and molar ratio $C_a/C_s = 0.2$.

a Poisson distribution was assumed, so that $\partial lnC_0/\partial lnC_a = -\overline{n}$, and the results are plotted versus volume fraction ϕ in Fig. 5.

For the Poisson distribution considered here, G_{aa} in the label limit is identical to that of the tracer limit, consistent with ideal mixing of solute labels within this hypothetical micellar solution. However, as shown in Fig. 5, the normalized cross terms of $[\mathbf{G}]$ are absent any effects from micelle growth, as expected, and thus do not vary with respect to volume fraction, as they do for the tracer limit.

4.6 Method of cumulants

The method of cumulants, which is often used to analyze dynamic light scattering data, is based on a general description of $g^{(1)}(q,\tau)$ for polydisperse solutions, expressed as a sum or integral of exponentials:[60]

$$g^{(1)}(q,\tau) = \int_0^\infty G(\Gamma)\, e^{-\Gamma\tau} d\Gamma\,, \tag{150}$$

where τ is a measurement time interval or time delay. Here, the integral defines a raw moment-generating function for the decay rate distribution $G(\Gamma)$, where Γ is a continuous decay rate variable. The logarithm of the integral in eqn (150) defines a cumulant generating function, which can be shown via a Taylor expansion of $e^{-\Gamma\tau}$ around $\Gamma\tau = 0$ to yield the following:

$$ln\{g^{(1)}(q,\tau)\} = -\bar{\Gamma}\tau + \frac{\kappa_2}{2}\tau^2 + \cdots\,. \tag{151}$$

In eqn (151), $\bar{\Gamma}$ and κ_2 are the first and second cumulants of $G(\Gamma)$, respectively. At infinite dilution, $G(\Gamma)$ for narrowly disperse hard sphere mixtures is monomodal with a mean $\bar{\Gamma} = q^2 D_z$ and variance $\kappa_2 = \overline{\Gamma^2} - \bar{\Gamma}^2$, defined via $\overline{\Gamma^m} = \int_0^\infty G(\Gamma)\,\Gamma^m d\Gamma$. The parameter D_z is the z-average diffusion coefficient, and the normalized second cumulant $\kappa_2/\bar{\Gamma}^2$ is used to provide an estimate for particle size polydispersity. However, at finite concentrations, $G(\Gamma)$ does not closely approximate the particle size distribution in general. This can be seen by merging eqn (26) with eqn (150). The resulting decay rate distribution for concentrated hard sphere dispersions,

$$G(\Gamma) = \left(\frac{1}{1+B}\right)\delta(\Gamma - \Gamma_+) + \left(\frac{B}{1+B}\right)\delta(\Gamma - \Gamma_-)\,, \tag{152}$$

is bimodal even if the particle size distribution is monomodal. In eqn (152), $\Gamma_+ = q^2 D_+$ and $\Gamma_- = q^2 D_-$ are the respective fast and slow mode decay rates. For concentrated solutions, the corresponding first and second cumulants of $G(\Gamma)$ can be directly related to parameters D_{DLS}, and $\kappa_2/\bar{\Gamma}^2$ that are routinely obtained when the method of cumulants analysis is applied to DLS measurements:

$$D_{DLS} = \frac{\bar{\Gamma}}{q^2} = \left(\frac{D_+ + BD_-}{1+B}\right)\,, \tag{153}$$

and

$$\frac{\kappa_2}{\bar{\Gamma}^2} = B\left(\frac{D_+ - D_-}{D_+ + BD_-}\right)^2\,. \tag{154}$$

Per eqn (153), the cumulant diffusivity D_{DLS} is a mode amplitude weighted average of eigenvalue diffusivities. Hence, D_+ is acquired via the cumulants analysis only when the slow mode amplitude is small relative to that of the fast mode, *i.e.*, when $B \ll 1$. Furthermore, the normalized second cumulant $\kappa_2/\bar{\Gamma}^2$ depends strongly on the difference $D_+ - D_-$, which increases with increasing ϕ for hard-sphere dispersions. Thus, $\kappa_2/\bar{\Gamma}^2$ for concentrated solutions does not solely depend on the variance of the particle size and refractive index distributions, in contrast to the case at infinite dilution.

5 Discussion

5.1 Driving forces for diffusion in the tracer and label limits

Within the framework of nonequilibrium thermodynamics,[61] the fluxes of solute (a) and surfactant (s) in a ternary mixture are linearly related to thermodynamic driving forces through a matrix of Onsager coefficients

$$\begin{bmatrix}\boldsymbol{J}_a\\ \boldsymbol{J}_s\end{bmatrix} = \begin{bmatrix}L_{aa} & L_{as}\\ L_{sa} & L_{ss}\end{bmatrix}\begin{bmatrix}\boldsymbol{X}_a\\ \boldsymbol{X}_s\end{bmatrix}\,. \tag{155}$$

If $\boldsymbol{J}_a$ and $\boldsymbol{J}_s$ are molar diffusive fluxes defined relative to a volume-fixed reference frame, then the conjugate, independent driving forces for diffusion can be expanded in terms of concentration gradients (see section 2.4 of SI)

$$-\begin{bmatrix}(\boldsymbol{X}_a)_{T,\mu_n}\\ (\boldsymbol{X}_s)_{T,\mu_n}\end{bmatrix} = \begin{bmatrix}(\boldsymbol{\nabla}\mu_a)_{T,\mu_n}\\ (\boldsymbol{\nabla}\mu_s)_{T,\mu_n}\end{bmatrix} = \begin{bmatrix}G_{aa} & G_{as}\\ G_{sa} & G_{ss}\end{bmatrix}\begin{bmatrix}\boldsymbol{\nabla}C_a\\ \boldsymbol{\nabla}C_s\end{bmatrix}\,. \tag{156}$$

Here, $(\boldsymbol{X}_a)_{T,\mu_n}$ and $(\boldsymbol{X}_s)_{T,\mu_n}$ are the driving forces for diffusion of the solute and surfactant, respectively, relative to a volume-fixed reference frame and the solvent is force-free according to $(\boldsymbol{X}_n)_{T,\mu_n} = -(\boldsymbol{\nabla}\mu_n)_{T,\mu_n} = \mathbf{0}$.

In the tracer limit, eqn (128)–(130) combine with eqn (156) to provide

$$\frac{C_a(\boldsymbol{X}_a)_{T,\mu_n}}{N_A k_B T} = -\nabla C_a\,, \tag{157}$$

and

$$\frac{C_s(\boldsymbol{X}_s)_{T,\mu_n}}{N_A k_B T} = \left[1 + \frac{3a_1}{m_1 R_1}\frac{(1+\phi+\phi^2)}{(1-\phi)^3} - \frac{V_a}{m_1 V_{hs}}\frac{(1+2\phi)^2}{(1-\phi)^4}\right]\nabla C_a - \frac{(1+2\phi)^2}{(1-\phi)^4}\nabla C_{tot}\,. \tag{158}$$

Eqn (157) describes a purely entropic thermodynamic driving force for the diffusion of solute in the tracer limit, identical to that predicted for solute diffusion in a dilute, binary mixture of solute and solvent. Furthermore, per eqn (157), surfactant gradients do not impose a driving force on the solute in the tracer limit, consistent with our previous results[9] for $[\mathbf{D}]$, which indicate that surfactant gradients do not drive coupled solute fluxes in the tracer limit ($D_{as} = 0$). However, according to eqn (158), the driving force acting on the surfactant is more complicated. The second term on the right-hand side of eqn (158) is an expected contribution to the surfactant thermodynamic force, indicating surfactant diffusion driven by gradients in the total micelle concentration, enhanced by a

factor that accounts for the influence of intermicellar interactions. The first term on the right-hand side of eqn (158) indicates that solute gradients also impose a driving force on the surfactant in a direction that points up the solute gradient. This contribution is enhanced by a term proportional to the micelle growth rate a_1 and is reduced by a term proportional to the molecular volume of the solute V_a. Again, this result is consistent with our previous predictions[9] for $[\mathbf{D}]$ in the tracer limit, which indicate uphill surfactant diffusion in response to a solute gradient in the tracer limit.

For the label case, eqn (139)–(141), and (156) combine to yield

$$\frac{\bar{n}(\boldsymbol{X}_a)_{T,\mu_n}}{N_A k_B T} = \frac{\partial ln C_1}{\partial ln C_a} \nabla ln\left(\frac{C_a}{C_s}\right) \tag{159}$$

and

$$\frac{m_1(\boldsymbol{X}_s)_{T,\mu_n}}{N_A k_B T} = -\frac{\partial ln C_1}{\partial ln C_a} \nabla ln\left(\frac{C_a}{C_s}\right) - \frac{d[\phi Z(\phi)]}{d\phi} \nabla ln C_{tot} \ . \tag{160}$$

According to eqn (159), solute label diffusion is driven exclusively by gradients in composition, per the so-called "exchange" or "self" or "interdiffusion" mode, which is purely entropic and depends on the distribution of solute within micelles via $\partial ln C_1/\partial ln C_a$. On the other hand, both gradients in composition and total micelle concentration contribute to the driving force on the surfactant within micelles according to eqn (160). The former contribution is interesting because, according to eqn (135), solute gradients do not drive coupled fluxes of surfactant in the label limit corresponding to $D_{sa} = 0$. However, per eqn (160), solute gradients do impose a driving force contribution on the surfactant, via the composition gradient $\nabla ln(C_a/C_s)$.

In order to understand this paradox, one may calculate the surfactant flux for mixtures at arbitrary concentration, $J_s = L_{sa}X_a + L_{ss}X_s$, by combining eqn (143), (144), (155), (159), and (160) to find

$$J_s = m_1 C_{tot}\left(\frac{D^0}{N_A k_B T}\right) K(\phi)\left[\bar{n}(\boldsymbol{X}_a)_{T,\mu_n} + m_1(\boldsymbol{X}_s)_{T,\mu_n}\right]. \tag{161}$$

Now, consider a solute gradient in the absence of a surfactant gradient, so that $\nabla C_s = 0$. Due to its label nature, a solute gradient has no ability to generate a total micelle concentration gradient in this scenario, since $\nabla ln C_{tot} = \nabla ln C_S = 0$. Hence, eqn (159) and (160) reduce to

$$\bar{n}(\boldsymbol{X}_a)_{T,\mu_n} = -m_1(\boldsymbol{X}_s)_{T,\mu_n} \ , \tag{162}$$

and, per eqn (161) and (162), $J_s = 0$. Physically, in the label limit, solute gradients (which entail composition gradients at uniform surfactant concentration) impose entropic forces on both the surfactant and the solute within micelles that are equal and opposite, producing a net zero force on micelles. Hence, composition gradients $\nabla ln(C_a/C_s)$ do not generate a net surfactant flux in the label limit, and act only to mix solute via the random motion of identically sized micelles in the absence of an overall micelle concentration gradient.

5.2 Multimodal analysis of $\left|g^{(1)}(q,t)\right|$

In Fig. 6, the logarithm of the field autocorrelation function $ln\left|g^{(1)}(q,\tau)\right|$ is plotted as a function of the time delay τ for binary $C_{12}E_{10}$/water mixtures, and ternary mixtures of either $C_{12}E_{10}$/decane/water or $C_{12}E_{10}$/limonene/water with $C_s = 200$mM and $C_a/C_s = 0.2$. Similarly, in Fig. 7, plots of $ln\left|g^{(1)}(q,\tau)\right|$ versus τ are provided for binary $C_{12}E_{10}$/water mixtures with $C_s = 20$, 200, and 400 mM. As shown in Fig. 6A and 7A, the data for dilute to moderately concentrated micellar solutions are linear with respect to time, indicating nearly monomodal decay of $\left|g^{(1)}(q,\tau)\right|$ up to $\phi = 0.25$. However, as shown in Fig. 7A, the profile is nonlinear when $C_s = 400$ mM,

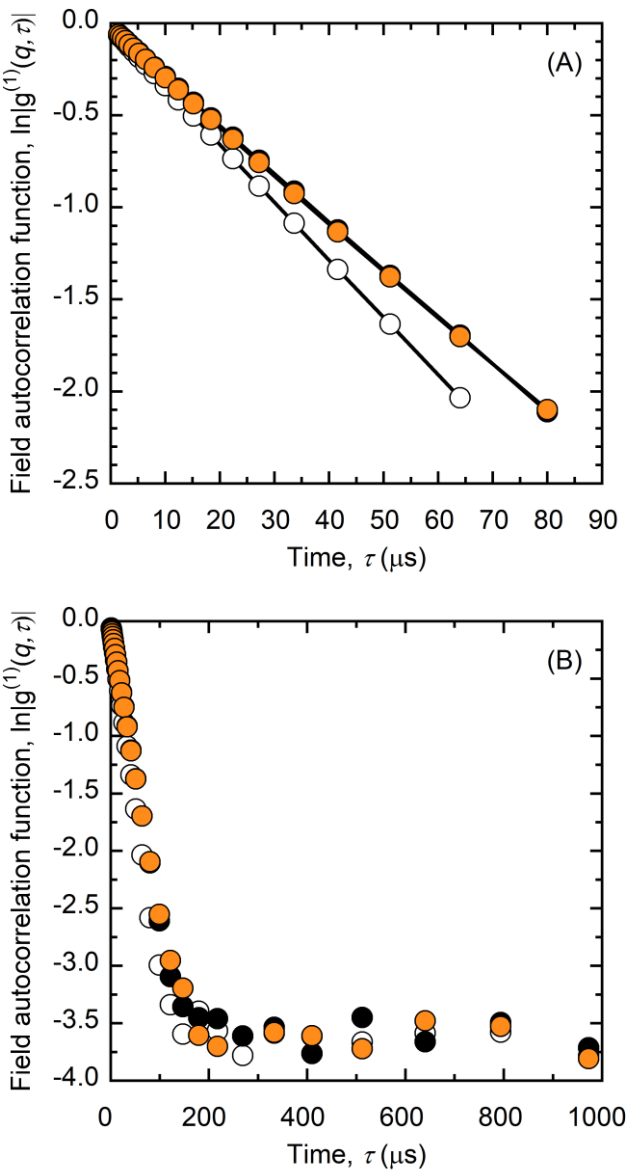

Fig. 6. Logarithm of the normalized field autocorrelation function $\left|g^{(1)}(q,\tau)\right|$ plotted as a function of time delay τ over 80 μs (A) and 1000 μs (B) for $C_{12}E_{10}$/water (open), $C_{12}E_{10}$/decane/water (black), and $C_{12}E_{10}$/limonene/water (orange) mixtures with $C_s = 200$mM, and $C_a/C_s = 0.2$ for ternary mixtures. The solid lines in (A) provide a guide for the eye, and error bars have been omitted for clarity.

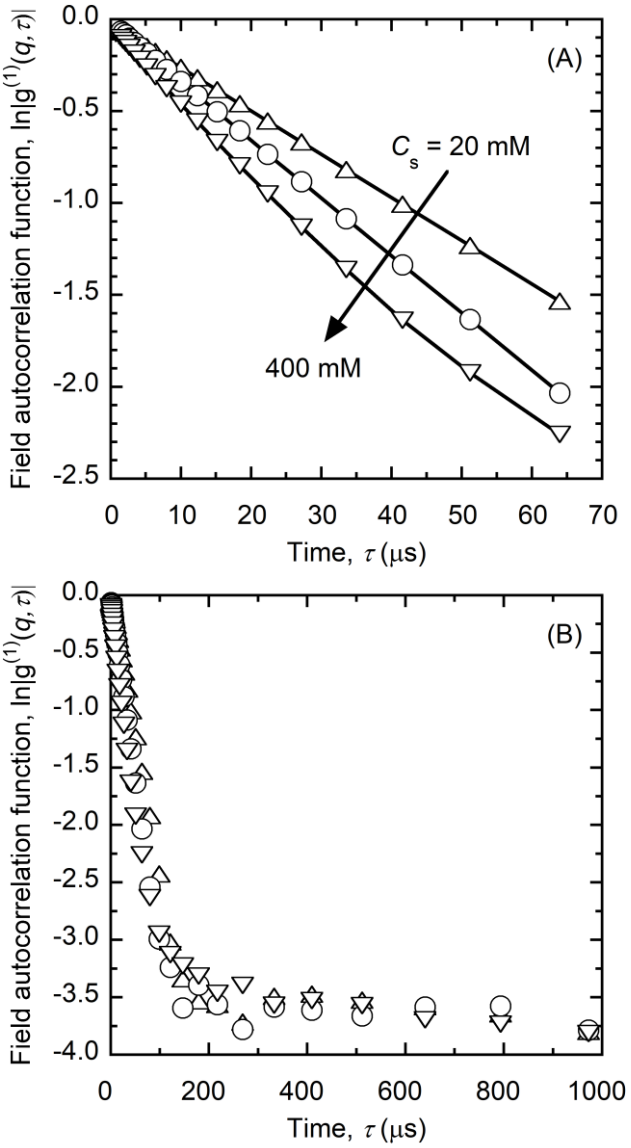

Fig. 7. The logarithm of the normalized field autocorrelation function $\left|g^{(1)}(q,\tau)\right|$ is plotted as a function of the time delay τ over 65 μs (A) and 1000 μs (B) for binary $C_{12}E_{10}$ (s)/water mixtures with $C_s = 20,\ 200$, and 400 mM. The solid lines in (A) provide a guide for the eye, and error bars have been omitted for clarity.

corresponding to $\phi = 0.53$. Similar results have been observed by others in concentrated ternary $C_{12}E_5$/decane/water[12] and binary $C_{12}E_8$/water systems.[62]

As discussed by Pusey et al.,[15] N decay modes for $\left|g^{(1)}(q,\tau)\right|$ are predicted for narrowly polydisperse colloidal mixtures with N different particle species, corresponding to the eigenvalues of the $N \times N$ particle diffusivity matrix. However, since the various exchange modes between different particle species cannot be resolved experimentally when the particle distribution is narrow, only two decay modes for $\left|g^{(1)}(q,\tau)\right|$, corresponding to long-time self and gradient diffusion, are prominent. As a result, the working model equation for DLS in a narrowly polydisperse colloidal mixture is identical to eqn (26), (83), and (84). Since D_+ is enhanced with increasing ϕ, the gradient term $1/(1+B)\,exp(-q^2 D_+ \tau)$ in eqn (26) at high ϕ decays quickly, revealing the slowly decaying self term $B/(1+B)\,exp(-q^2 D_- \tau)$ when $\tau \gg 1/(q^2 D_+)$. For some systems, such as ternary water–in–oil microemulsions of AOT/water/octane,[44] two decay modes (slopes) are distinct in a plot of $ln\left|g^{(1)}(q,\tau)\right|$ versus τ, which enables a robust fit using eqn (26).

The nonlinearity (slight upturn) in $ln\left|g^{(1)}(q,\tau)\right|$ versus τ in Fig. 7A for concentrated mixtures of solute-free micelles with $C_s = 400$ mM could indicate the emergence of an average self mode, resulting from optical and size polydispersity between micelles with various aggregation numbers. However, the upturn is only slight and in Fig. 7B measurement noise appears to overtake the signal before the self mode can establish itself, preventing access to the long–time self diffusivity predicted by eqn (83). Hence, in this study, we found our data could be more robustly analyzed using the method of cumulants (*i.e.,* eqn (151)), in lieu of a multiexponential fit, even at high concentrations.

5.3 Diffusion coefficients measured by DLS for $C_{12}E_{10}$/solute/water mixtures

In this section, DLS diffusivities, acquired using the method of cumulants for ternary, nonionic micellar solutions with hydrophobic solutes, are compared with theory for gradient diffusion in dilute and concentrated monodisperse colloidal dispersions. As discussed in section 4.4, the mode amplitude ratio $B = 0$ for locally monodisperse micellar solutions, so that eqn (84), (91), and (153) combine to provide the following

$$\frac{D_{DLS}}{D_{i^*}^0} = 1 + (f+h)\phi + L\phi^2\,. \qquad (163)$$

Eqn (163) indicates that DLS measurements, analyzed via the method of cumulants, are predicted to yield micelle gradient diffusion coefficients. For concentrated, monodisperse hard sphere dispersions, the gradient diffusion coefficient D_c can be expressed via the following form of the generalized Stokes-Einstein equation,[38, 63, 64]

$$\frac{D_c}{D^0} = \frac{K(\phi)}{S^I(\phi)} = K(\phi)\phi\left(\frac{\partial\mu}{\partial\phi}\right)_{T,\mu_n}\,. \qquad (164)$$

Here, $S^I(\phi)$ is the ideal static structure factor in the low wavevector limit $qR_{i^*} \to 0$ and $K(\phi)$ is the bulk mobility coefficient. Rigorous theoretical results for $K(\phi)$, applicable to dilute mixtures of colloidal hard spheres, have been derived accounting for pairwise[65] and three-body[66] hydrodynamic interactions. For concentrated hard sphere dispersions, numerical simulations that include many-body hydrodynamic interactions have also been performed to determine $K(\phi)$ using either Stokesian dynamics[67] or the lattice Boltzmann method.[68]

In Fig. 8A, normalized gradient diffusion coefficients D_{DLS}/D_{DLS}^0 are plotted versus ϕ for $C_{12}E_{10}$/water, and for $C_{12}E_{10}$/limonene/water, and $C_{12}E_{10}$/limonene/decane[8] mixtures with $C_a/C_s = 0.2$. The experimental values are compared with dilute theory by Batchelor[38] (solid line) for monodisperse hard

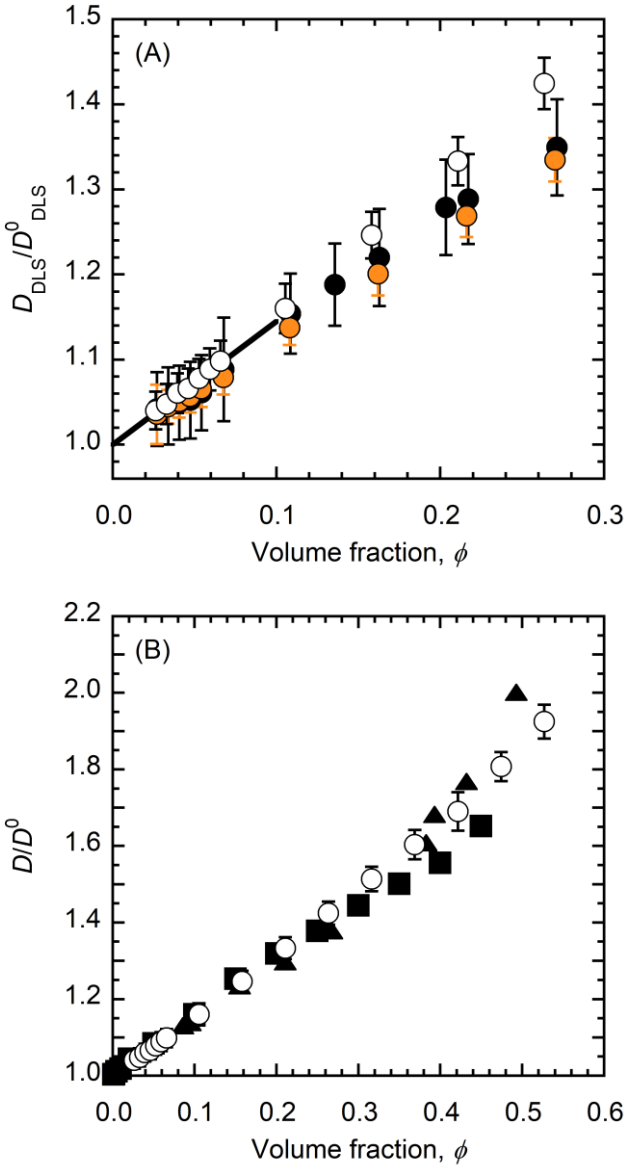

Fig. 8. (A) Normalized diffusion coefficients for $C_{12}E_{10}$/water (open circles), $C_{12}E_{10}$/decane/water[8] (black circles), and $C_{12}E_{10}$/limonene/water (orange circles) with $C_a/C_s = 0.2$ as a function of volume fraction, superimposed with theoretical predictions by Bachelor[38] for dilute, monodisperse hard-sphere dispersions (solid line). (B) Normalized diffusion coefficients for concentrated $C_{12}E_{10}$/water mixtures (open circles) with numerical simulation results for crowded hard sphere dispersions calculated using Stokesian Dynamics[67] (squares) and the Lattice Boltzmann method[68] (triangles). Error bars indicate 95% confidence intervals.

sphere dispersions, *i.e.,* using $D_c/D^0 = 1.45\phi$. In addition, D_{DLS}/D^0_{DLS} values are plotted as a function of ϕ in Fig. 8B for binary $C_{12}E_{10}$/water mixtures up to $\phi = 0.53$, superimposed with numerical results for concentrated monodisperse hard sphere suspensions. Micelle volume fractions were calculated using

$$\phi = C_a\bar{V}_a + C_s(\bar{V}_s + n_H\bar{V}_w)\,, \qquad (165)$$

where the molar volumes for the solute (a) and water (w) are given by $\bar{V}_a = MW_a/\rho_a$ and $\bar{V}_w = MW_w/\rho_w$, respectively, with MW_a, MW_w, ρ_a, and ρ_w indicating the respective molecular weights and pure component densities. The dry $C_{12}E_{10}$ surfactant molar volume was interpolated from density data for a homologous series of $C_{12}E_m$ surfactants.[47] Molar volume calculations for decane, limonene, dry C12E10 surfactant, and water yield $\bar{V}_a = 1.949 \times 10^{-4}\, mM^{-1}$, $\bar{V}_a = 1.622 \times 10^{-4}\, mM^{-1}$, $\bar{V}_s = 5.968 \times 10^{-4}\, mM^{-1}$, and $\bar{V}_w = 1.802 \times 10^{-5}\, mM^{-1}$, respectively. In addition, the conversion factor $6.022 \times 10^{-4}\ (nm^3/molecule)/mM$ was used in this work to convert between molecular and molar volume.

Numerical calculations were performed using the Carnahan-Starling equation[58] for the ideal static structure factor in eqn (164), and results for $K(\phi)$ were determined from numerical simulations via either Stokesian dynamics[67] (squares) or the lattice Boltzmann method method[68] (triangles). As shown in Fig. 8, solute-free, decane-containing, and limonene-containing $C_{12}E_{10}$ micelles diffused as hard spheres in accordance with the most rigorous theoretical results available for gradient diffusion in dilute and concentrated colloidal hard sphere dispersions. Furthermore, as noted by others,[68, 69] Batchelor's dilute theory[38] provides an excellent approximation for D_c/D^0 for concentrated monodisperse hard sphere dispersions up to $\phi \approx 0.4$, indicating a near cancellation of higher order, many body hydrodynamic and thermodynamic virial contributions.

5.4 Rayleigh ratios for $C_{12}E_{10}$/solute/water mixtures

Neglecting local micelle polydispersity, theoretical predictions for the Rayleigh ratio for binary $C_{12}E_{10}$/water and ternary $C_{12}E_{10}$/solute/water mixtures were calculated using eqn (93) and (94) with $V_{hs} = 2.19\text{nm}^{-3}$, $V_a = 0.32\text{nm}^{-3}$ (decane) or 0.26nm^{-3} (limonene), and $\lambda_0 = 633\text{nm}$. The refractive indices were determined via $n = (\partial n/\partial\phi)_{p,T,C_a/C_s}\phi + n_0$ with $n_0 = 1.33$ and $(\partial n/\partial\phi)_{p,T,C_a/C_s} = 0.063$, 0.064, and 0.065 for solute-free, decane and limonene containing micelles, respectively. Average micelle volumes were calculated from DLS data using $V_{i^*} = 4/3\,\pi {R_{DLS}}^3$, where hydrodynamic radii for solute-free, decane, and limonene-containing micelles are given by $R_{DLS} = 3.75$ nm, 4.25 nm, and 4.04 nm, respectively.

In Fig. 9, R_{90} results for $C_{12}E_{10}$/water (open circles), $C_{12}E_{10}$/decane/water (black), and $C_{12}E_{10}$/limonene/water (orange) mixtures are compared with these theoretical predictions derived using thermodynamic fluctuation theory (solid lines) as a function of ϕ. As shown, the experimental data for both binary and ternary mixtures is in excellent agreement with theoretical predictions up to $\phi = 0.3$, indicating that $C_{12}E_{10}$ micelles interacted as hard spheres, regardless of the presence of decane or limonene solubilizate. These results are consistent with those reported for similar systems, including $C_{12}E_8$/water[62, 70] and $C_{12}E_5$/decane/water.[12]

5.5 Effect of crowding on micelle hydration

As shown in Fig. 9, eqn (93) and (94) appear to underestimate R_{90} for binary aqueous $C_{12}E_{10}$ mixtures when $\phi > 0.3$, to an extent that increases with increasing ϕ. To explain this effect, we note that micelle dehydration has been observed in aqueous $C_{12}E_8$ solutions at high concentrations $\phi > 0.3$ using NMR,[71] and in dilute aqueous C_8E_5 solutions at

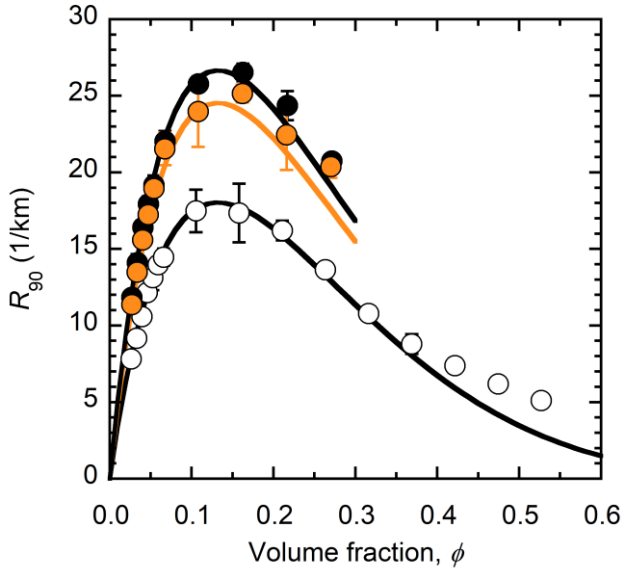

Fig. 9. Rayleigh ratios plotted versus ϕ for $C_{12}E_{10}$/water (open circles) and $C_{12}E_{10}$/decane/water (black) and $C_{12}E_{10}$/limonene/water (orange) mixtures with $C_a/C_s = 0.2$. Theoretical predictions calculated using eqn (93) and (94) for binary and ternary solutions are shown as solid curves. Error bars indicate two standard deviations.

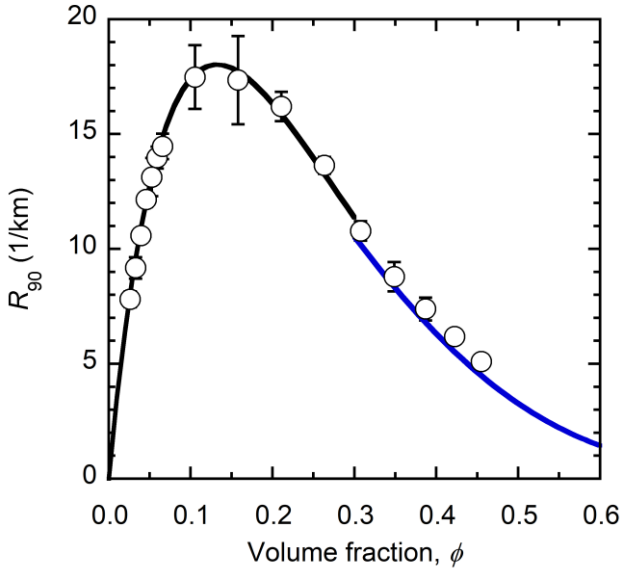

Fig. 10. Rayleigh ratios for binary, aqueous $C_{12}E_{10}$ solutions plotted versus the micelle volume fraction. Values for $\phi > 0.3$ were calculated assuming linear dehydration according to $n_H = 50 - C_s/20$, where C_s has (mM) units. Theoretical predictions indicated by the solid curves were calculated using either eqn (93) and (94) (black curve) or eqn (165)–(168) (blue curve).

high pressures up to 310 MPa via SANS.[72] These results indicate that, unlike hard spheres, hydrated micelles tend to relax the system free energy by reducing their size, and thus the volume fraction of the mixture, via dehydration. In order to capture the influence of dehydration on our theoretical predictions for the Rayleigh ratio, we use thermodynamic fluctuation theory to derive R_{90} for a binary mixture of hydrated surfactant (s) and water with a concentration dependent hydration index $n_H = n_H(T, p, C_s)$ (see section 3.5 of SI)

$$R_{90} = \frac{4\pi^2 n^2}{{\lambda_0}^4} \frac{\left(\frac{\partial n}{\partial C_s}\right)_{p,T}^2}{\left[1 + {C_s}^2 \bar{V}_w \left(\frac{\partial n_H}{\partial C_s}\right)_{p,T}\right]} \frac{C_s m_1}{N_A} \left\{\frac{d[C_s Z(\phi)]}{dC_s}\right\}^{-1} . \quad (166)$$

In eqn (166), the refractive index increment is given by

$$\left(\frac{\partial n}{\partial C_s}\right)_{T,p} = \left(\frac{\partial n}{\partial C_s}\right)_{p,T,n_H} + \left(\frac{\partial n}{\partial n_H}\right)_{p,T,C_s} \left(\frac{\partial n_H}{\partial C_s}\right)_{p,T} , \quad (167)$$

and, using eqn (94) for the Carnahan-Starling compressibility factor, we have

$$\frac{d[C_s Z(\phi)]}{dC_s} = \frac{(1+2\phi)^2 - \phi^3(4-\phi)}{(1-\phi)^4} - {C_s}^2 \bar{V}_w \left(\frac{\partial n_H}{\partial C_s}\right)_{p,T} \frac{(4+4\phi-2\phi^2)}{(1-\phi)^4} , \quad (168)$$

Per eqn (165)–(168), micelle dehydration affects the Rayleigh ratio in several ways via terms involving the hydration index derivative $(\partial n_H/\partial C_s)_{T,p}$. According to Nilsson et al.[71] the hydration index for $C_{12}E_8$ micelles decreases linearly with surfactant concentration with a slope approximately equal to $(\partial n_H/\partial C_s)_{T,p} = -1/20\, mM^{-1}$ when $\phi > 0.3$. Furthermore, n_H is expected to remain unchanged with ϕ at lower concentrations, suggesting one may use eqn (93) and (94) with constant n_H to predict R_{90} for $\phi \leq 0.3$.

Using eqn (165)–(168) with $\bar{V}_s = 5.968 \times 10^{-4}\, mM^{-1}$, $\bar{V}_w = 1.802 \times 10^{-5}\, mM^{-1}$, $(\partial n/\partial C_s)_{T,p} \approx (\partial n/\partial C_s)_{T,p,n_H} = 8.24 \times 10^{-5}\, mM^{-1}$, $(\partial n_H/\partial C_s)_{T,p} = -1/20\, mM^{-1}$, $m_1 = 103$, and $n_H = 50 - C_s/20$, in accordance with refractive index data by us and NMR data by Nilsson et al.,[71] theoretical predictions for Rayleigh ratios and volume fractions for binary aqueous $C_{12}E_{10}$ solutions were re-calculated and plotted against the new values for $\phi > 0.3$ in Fig. 10. As shown, good agreement is achieved, indicating dehydration is a likely explanation for the discrepancy in R_{90} between our data for binary $C_{12}E_{10}$/water mixtures and monodisperse hard sphere theory. In addition, we note that dehydration does not significantly affect the slope of the normalized solute-free DLS diffusivities shown in Fig. 8B, since values for ϕ and D^0 corrected for dehydration are reduced and enhanced, respectively, causing the DLS data points above $\phi > 0.3$ in Fig. 8A to shift left and down.

6 Conclusions

The self-assembled nature of aqueous micellar solutions comprised of nonionic surfactants and hydrophobic solutes may drive strong micelle growth as these molecules reassemble in response to variations in composition, thereby distinguishing these mixtures from rigid particle dispersions. These effects were previously demonstrated to have a strong effect on the ternary diffusivity matrix $[\mathbf{D}]$, via the function $M(\phi, C_a/C_s)$. In this work, however, micelle growth effects are shown to have no influence on the either the Rayleigh ratio or the field correlation function in the limit of zero local micelle polydispersity. In particular, theoretical predictions for the field

autocorrelation function $\left|g^{(1)}(\boldsymbol{q},t)\right|$ decay according to the larger eigenvalue, regardless of the relative scattering power of the components in the mixture, corresponding to pure gradient diffusion of monodisperse, interacting hard spheres.

These results suggest that light scattering theory, developed for monodisperse, colloidal hard sphere dispersions, applies to narrowly polydisperse, ternary solutions comprised of solute-containing micelles. Furthermore, rigorous theoretical results in the tracer limit for the thermodynamic derivatives and the driving forces for diffusion, display the influence of micelle growth/self-assembly effects and show that the diffusional transport processes, which occur during light scattering measurements, are different from those of binary, monodisperse colloidal dispersions comprised of rigid spheres.

Author Contributions

Nathan P. Alexander: Conceptualization (lead), Formal analysis (lead), Investigation (lead), Writing—original draft (lead), Writing—review and editing (supporting). **Ronald J. Phillips**: Conceptualization (supporting), Formal analysis (supporting), Funding acquisition (equal), Supervision (supporting), Writing—review and editing (supporting). **Stephanie R. Dungan**: Conceptualization (supporting), Formal analysis (supporting), Funding acquisition (equal), Supervision (lead), Writing—review and editing (lead).

Conflicts of interest

There are no conflicts of interest to declare.

Acknowledgements

This research was funded by the National Science Foundation (CBET1506474), and from Hatch project 1010420, from the USDA National Institute of Food and Agriculture. N. P. A. acknowledges a Graduate Assistance in Areas of National Need (GAANN) fellowship from the University of California at Davis. All authors gratefully acknowledge Ulf Nobbmann from Malvern for allowing us to borrow a light scattering apparatus for an extended period.

References

1. L. Onsager, Reciprocal Relations in Irreversible Processes. I., *Phys. Rev.*, 1931, **37**, 405–426.
2. L. Onsager, Reciprocal Relations in Irreversible Processes. II., *Phys. Rev.*, 1931, **38**, 2265–2279.
3. R. Aris, On the Dispersion of a Solute in a Fluid Flowing through a Tube, *Proc. R. Soc. London, Ser. A*, 1956, **235**, 67–77.
4. W. E. Price, Theory of the Taylor Dispersion Technique for 3-Component-System Diffusion Measurements, *J. Chem. Soc., Faraday Trans. 1*, 1988, **84**, 2431–2439.
5. G. Taylor, Dispersion of Soluble Matter in Solvent Flowing Slowly through a Tube, *Proc. R. Soc. London, Ser. A*, 1953, **219**, 186–203.
6. W. J. Musnicki, S. R. Dungan and R. J. Phillips, Multicomponent Diffusion in Solute-Containing Micelle and Microemulsion Solutions, *Langmuir*, 2014, **30**, 11019–11030.
7. W. A. Wakeham, A. Nagashima and J. V. Sengers, *Measurement of the transport properties of fluids*, Blackwell Scientific Publications, 1991.
8. N. P. Alexander, R. J. Phillips and S. R. Dungan, Multicomponent Diffusion in Aqueous Solutions of Nonionic Micelles and Decane, *Langmuir*, 2019, **35**, 13595–13606.
9. N. P. Alexander, R. J. Phillips and S. R. Dungan, Multicomponent Diffusion of Interacting, Nonionic Micelles with Hydrophobic Solutes, *Soft Matter*, 2021, **17**, 531–542.
10. M. A. Budroni, J. Carballido-Landeira, A. Intiso, A. De Wit and F. Rossi, Interfacial Hydrodynamic Instabilities Driven by Cross-Diffusion in Reverse Microemulsions, *Chaos*, 2015, **25**.
11. D. G. Leaist, Relating Multicomponent Mutual Diffusion and Intradiffusion for Associating Solutes. Application to Coupled Diffusion in Water-in-oil Microemulsions, *Phys. Chem. Chem. Phys.*, 2002, **4**, 4732–4739.
12. U. Olsson and P. Schurtenberger, Structure, Interactions, and Diffusion in a Ternary Nonionic Microemulsion near Emulsification Failure, *Langmuir*, 1993, **9**, 3389–3394.
13. U. Olsson and P. Schurtenberger, A Hard Sphere Microemulsion, *Prog. Colloid Polym. Sci.*, 1997, **104**, 157–159.
14. W. L. Griffith, R. Triolo and A. L. Compere, Analytical Scattering Function of a Polydisperse Percus-Yevick Fluid with Schulz-(Gamma-) Distributed Diameters, *Phys. Rev. A*, 1987, **35**, 2200–2206.
15. P. N. Pusey, H. M. Fijnaut and A. Vrij, Mode Amplitudes in Dynamic Light-Scattering by Concentrated Liquid Suspensions of Polydisperse Hard-Spheres, *J. Chem. Phys.*, 1982, **77**, 4270–4281.
16. A. Van Veluwen, H. N. W. Lekkerkerker, C. G. de Kruif and A. Vrij, Influence of Polydispersity on Dynamic Light-Scattering Measurements on Concentrated Suspensions, *J. Chem. Phys.*, 1988, **89**, 2810–2815.
17. A. Vrij, Light-Scattering of a Concentrated Multicomponent System of Hard Spheres in Percus-Yevick Approximation, *J. Chem. Phys.*, 1978, **69**, 1742–1747.
18. A. Vrij, Concentrated, Polydisperse Solutions of Colloidal Particles—Light-Scattering and Sedimentation of Hard-Sphere Mixtures, *J. Colloid Interface Sci.*, 1982, **90**, 110–116.
19. M. Nayeri, M. Zackrisson and J. Bergenholtz, Scattering Functions of Core-Shell-Structured Hard Spheres with Schulz-Distributed Radii, *J. Phys. Chem. B*, 2009, **113**, 8296–8302.
20. Y. D. Yan and J. H. R. Clarke, Dynamic Light-Scattering from Concentrated Water-in-Oil Microemulsions the Coupling of Optical and Size Polydispersity, *J. Chem. Phys.*, 1990, **93**, 4501–4509.
21. A. Bardow, On the Interpretation of Ternary Diffusion Measurements in Low-Molecular Weight Fluids by Dynamic Light Scattering, *Fluid Phase Equilib.*, 2007, **251**, 121–127.

22. B. J. Berne and R. Pecora, in *Dynamic light scattering : with applications to chemistry, biology, and physics*, Wiley, New York, 1976, ch. 10, pp. 263–272.
23. L. Blum, Light Scattering from Multicomponent Fluids, *J. Chem. Phys.*, 1969, **50**, 17–20.
24. J. G. Kirkwood and R. J. Goldberg, Light Scattering Arising from Composition Fluctuations in Multi-Component Systems, *J. Chem. Phys.*, 1950, **18**, 54–57.
25. R. D. Mountain and J. M. Deutch, Light Scattering from Binary Solutions, *J. Chem. Phys.*, 1969, **50**, 1103–1108.
26. W. H. Stockmayer, Light Scattering in Multi-Component Systems, *J. Chem. Phys.*, 1950, **18**, 58–61.
27. F. Zernike, L'Opalescence Critique, *Dissertation*, Amsterdam, 1915.
28. H. C. Brinkman and J. J. Hermans, The Effect of Non-Homogeneity of Molecular Weight on the Scattering of Light by High Polymer Solutions, *J. Chem. Phys.*, 1949, **17**, 574–576.
29. S. R. de Groot and P. Mazur, in *Non-equilibrium thermodynamics*, Dover Publications, New York, Dover edn., 1984, ch. VII, pp. 83–129.
30. H. N. W. Lekkerkerker and W. G. Laidlaw, Spectral analysis of the light scattered by a ternary mixture, *J. Chem. Soc., Faraday Trans. 2*, 1974, **70**, 1088.
31. H. N. W. Lekkerkerker and W. G. Laidlaw, Onsager Symmetry Relations and the Spectral Distribution of Scattered Light, *Phys. Rev. A*, 1972, **5**, 1604–1607.
32. H. N. W. Lekkerkerker and W. G. Laidlaw, Spectral Analysis of Light Scattered from Fluids, *Phys. Rev. A*, 1973, **7**, 1332–1339.
33. J. P. Boon and S. Yip, in *Molecular hydrodynamics*, Dover Publications, New York, Dover edn., 1991, ch. 5, pp. 237–276.
34. J. M. Ortiz de Zárate and J. V. Sengers, in *Hydrodynamic fluctuations in fluids and fluid mixtures*, Elsevier, 1st edn., 2006, ch. 3, pp. 39–62.
35. J. M. Ortiz de Zárate, J. L. Hita and J. V. Sengers, Fluctuating Hydrodynamics and Concentration Fluctuations in Ternary Mixtures, *C. R. Mec.*, 2013, **341**, 399–404.
36. J. M. Ortiz de Zárate and J. V. Sengers, in *Experimental thermodynamics volume X: non-equilibrium thermodynamics with applications*, Royal Society of Chemistry, 2015, ch. 2, pp. 21–38.
37. S. R. de Groot and P. Mazur, in *Non-equilibrium thermodynamics*, Dover Publications, New York, Dover edn., 1984, ch. III, p. 23.
38. G. K. Batchelor, Brownian Diffusion of Particles with Hydrodynamic Interaction, *J. Fluid Mech.*, 1976, **74**, 1–29.
39. G. K. Batchelor, Diffusion in a Dilute Polydisperse System of Interacting Spheres, *J. Fluid Mech.*, 1983, **131**, 155–175.
40. G. K. Batchelor, Corrigendum, *J. Fluid Mech.*, 1983, **137**, 467–469.
41. B. Das, B. Maitra, S. M. Mercer, M. Everist and D. G. Leaist, A Comparison of Diffusion Coefficients for Ternary Mixed Micelle Solutions Measured by Macroscopic Gradient and Dynamic Light Scattering Techniques, *Phys. Chem. Chem. Phys.*, 2008, **10**, 3083–3092.
42. D. G. Leaist and L. Hao, Comparison of Diffusion-Coefficients of Multicomponent Solutions from Light-Scattering and Macroscopic Gradient Techniques—Sodium Dodecyl-Sulfate Micelles in Aqueous Salt-Solutions, *J. Phys. Chem.*, 1993, **97**, 7763–7768.
43. A. Shukla and R. H. H. Neubert, Diffusion Behavior of Pharmaceutical O/W Microemulsions Studied by Dynamic Light Scattering, *Colloid Polym. Sci.*, 2006, **284**, 568–573.
44. A. Shukla, H. Graener and R. H. H. Neubert, Observation of Two Diffusive Relaxation Modes in Microemulsions by Dynamic Light Scattering, *Langmuir*, 2004, **20**, 8526–8530.
45. O. Annunziata, D. Buzatu and J. G. Albright, Protein diffusion coefficients determined by macroscopic-gradient Rayleigh interferometry and dynamic light scattering, *Langmuir*, 2005, **21**, 12085–12089.
46. P. Schurtenberger, in *Light scattering: principles and development*, ed. W. Brown, Oxford University Press, Oxford, 1996, ch. 9, pp. 293–326.
47. S. Kaneshina, M. Yoshimoto, H. Kobayashi, N. Nishikido, G. Sugihara and M. Tanaka, Effect of Pressure on Apparent Molal Volumes of Non-Ionic Surfactants in Aqueous-Solutions, *J. Colloid Interface Sci.*, 1980, **73**, 124–129.
48. Y. Tokuoka, H. Uchiyama, M. Abe and K. Ogino, Solubilization of Synthetic Perfumes by Nonionic Surfactants, *J. Colloid Interface Sci.*, 1992, **152**, 402–409.
49. S. Vafaei, B. Tomberli and C. G. Gray, McMillan-Mayer Theory of Solutions Revisited: Simplifications and Extensions, *J. Chem. Phys.*, 2014, **141**, 1–18.
50. W. G. McMillan and J. E. Mayer, The Statistical Thermodynamics of Multicomponent Systems, *J. Chem. Phys.*, 1945, **13**, 276–305.
51. B. J. Berne and R. Pecora, in *Dynamic light scattering : with applications to chemistry, biology, and physics*, Wiley, New York, 1976, ch. 4, pp. 40–42 and 48–50.
52. B. J. Berne and R. Pecora, in *Dynamic light scattering : with applications to chemistry, biology, and physics*, Wiley, New York, 1976, ch. 3, pp. 25–28.
53. B. J. Berne and R. Pecora, in *Dynamic light scattering : with applications to chemistry, biology, and physics*, Wiley, New York, 1976, ch. 11, pp. 298–302.
54. J. M. Rallison and E. J. Hinch, The Effect of Particle Interactions on Dynamic Light-Scattering from a Dilute Suspension, *J. Fluid Mech.*, 1986, **167**, 131–168.
55. S. R. de Groot and P. Mazur, in *Non-equilibrium thermodynamics*, Dover Publications, New York, Dover edn., 1984, ch. XI, pp. 246–262.
56. G. K. Batchelor, Note on the Onsager Symmetry of the Kinetic Coefficients for Sedimentation and Diffusion in a Dilute Bidispersion, *J. Fluid Mech.*, 1986, **171**, 509–517.
57. B. C. Stephenson, A. Goldsipe, K. J. Beers and D. Blankschtein, Quantifying the Hydrophobic Effect. 1. A Computer Simulation-Molecular-Thermodynamic Model for the Self-Assembly of Hydrophobic and Amphiphilic Solutes in Aqueous Solution, *J. Phys. Chem. B*, 2007, **111**, 1025–1044.
58. N. F. Carnahan and K. E. Starling, Equation of State for Nonattracting Rigid Spheres, *J. Chem. Phys.*, 1969, **51**, 635–636.
59. T. Hill, in *An introduction to statistical thermodynamics*, Addison-Wesley Publishing Company, Inc., United States, 2nd edn., 1960, ch. 19, pp. 340–368.
60. D. E. Koppel, Analysis of Macromolecular Polydispersity in Intensity Correlation Spectroscopy—Method of Cumulants, *J. Chem. Phys.*, 1972, **57**, 4814–-4820.
61. S. R. de Groot and P. Mazur, in *Non-equilibrium thermodynamics*, Dover Publications, New York, Dover edn., 1984, ch. IV, pp. 30–31.

62. M. Imai, M. Kurimoto, F. Matsuura, Y. Sakuma and T. Kawakatsu, Diffusion of Surfactant Micelles in Fluid and Crystal Phases, *Soft Matter*, 2012, **8**, 9892–9905.
63. W. B. Russel and A. B. Glendinning, The Effective Diffusion-Coefficient Detected by Dynamic Light-Scattering, *J. Chem. Phys.*, 1981, **74**, 948–952.
64. W. B. Russel, D. A. Saville and W. R. Schowalter, *Colloidal dispersions*, Cambridge University Press, Cambridge ; New York, 1989.
65. G. K. Batchelor, Sedimentation in a Dilute Dispersion of Spheres, *J. Fluid Mech.*, 1972, **52**, 245–268.
66. B. Cichocki, M. L. Ekiel-Jezewska, P. Szymczak and E. Wajnryb, Three-particle Contribution to Sedimentation and Collective Diffusion in Hard-Sphere Suspensions, *J. Chem. Phys.*, 2002, **117**, 1231–1241.
67. A. J. C. Ladd, Hydrodynamic Transport-Coefficients of Random Dispersions of Hard-Spheres, *J. Chem. Phys.*, 1990, **93**, 3484–3494.
68. P. N. Segre, O. P. Behrend and P. N. Pusey, Short-Time Brownian-Motion in Colloidal Suspensions—Experiment and Simulation, *Phys. Rev. E*, 1995, **52**, 5070–5083.
69. A. J. Banchio and G. Nagele, Short-time Transport Properties in Dense Suspensions: From Neutral to Charge-Stabilized Colloidal Spheres, *J. Chem. Phys.*, 2008, **128**.
70. M. Corti, Degiorgio, V., Hayter, J. B., Zulauf, M., Micelle Structure in Isotropic $C_{12}E_8$ Amphiphile Solutions., *Chem. Phys. Lett.*, 1984, **109**, 579–583.
71. P. G. Nilsson and B. Lindman, Water Self-Diffusion in Non-Ionic Surfactant Solutions—Hydration and Obstruction Effects, *J. Phys. Chem.*, 1983, **87**, 4756–4761.
72. M. Lesemann, H. Nathan, T. P. DiNoia, C. F. Kirby, M. A. McHugh, J. H. van Zanten and M. E. Paulaitis, Self-assembly at High Pressures: SANS Study of the Effect of Pressure on Microstructure of C_8E_5 Micelles in Water, *Ind. Eng. Chem. Res.*, 2003, **42**, 6425–6430.